Dear editor,

Please find bellow our responses to the reviewers' valuable comments regarding the manuscript entitled "TEMIS UV product validation using NILU-UV ground-based measurements in Thessaloniki, Greece".

For better readability, the reviewers' comments are highlighted in bold while our responses are provided in blue. All pertinent changes are included in our point-by-point answers.

At the end of the document, we also provide the marked-up revised version.

Sincerely,

Dr. Melina Zempila.

<u>Reviewer #1: Comments and Suggestions</u>

Some rationale should be provided why TEMIS data were evaluated with NILU-UV measurements and not directly with Brewer measurements, which should be the most accurate. While the calibration of NILU-UV measurements against the Brewer measurement with the NN technique is a very interesting novel approach, it involves an extra step leading to an increase in the uncertainty of ground-based measurements.
I realize that that NILU-UV data have much larger temporal resolution than Brewer measurements but it is not clear whether this is important considering that only daily dose data from TEMIS were evaluated. For example, are there large gaps in Brewer measurements, which would favor the NILU-UV data set? Is there an analysis that shows that the high temporal resolution of the NILU-UV data is critical for satellite data validation?

We agree that Brewer data provide higher accuracy since, as the reviewer indicates, NILU data also include the uncertainty of the NN retrieval. However, for this study in order to evaluate the TEMIS daily doses we used data of 10-minute time intervals, the time resolution of the TEMIS UV dose time integration. NILU provides data with the necessary time resolution in order to acquire higher number of coincidences at the exact time of the TEMIS model estimation during a day. Unfortunately, Brewer's time frequency spans from 20 to 40 minutes (page 6 / line 23). Under cloudy conditions, this higher time resolution is considered more beneficiary for the accuracy of the comparisons. Thus, we chose to use NILU data in order to have a daily representative value.
To make this clear we also added a short description on page 8, lines: 3-4. We hope that this is sufficient.

"The B086 provides measurements with a time frequency of 20 to 40 minutes, but atmospheric circumstances can change considerably within this period. It is therefore better to base the evaluation of the TEMIS UV dose rate (available at 10-minute intervals) on the NILU103 data, which have a better temporal resolution; thus they suffer much less from changes in atmospheric conditions (like clouds) during one measurement than the Brewer measurements."

Differences between instruments are often given with a 0.01% precision. Considering that the uncertainties of all datasets are much larger, I suggest to round percentages to 0.1% throughout the paper, including the figures. This would also improve the readability of the text.

We thank you for the suggestion. We updated all pertinent graphs and text accordingly.

<u>Specific comments</u>

P2, L7: The sentence "Furthermore..." is confusing. It implies that the production of Vitamin D is detrimental. Mention the benefits of Vitamin D and then discuss that there may be an ideal UV exposure, which balances the harmful and beneficial effects of UV radiation!

We rephrased the sentence to "On the other hand, the cutaneous production of vitamin D, a 'vitamin' that is proven to be essential for human health, is also activated by spectral UV radiation.

Hence accurate knowledge of 'safe' UV doses for humans is paramount in order to balance the harmful and beneficial effects of UV exposure."

P3, L30: I note that the 1987 CIE norm for the UV index has been updated. See: Webb, Ann R., Harry Slaper, Peter Koepke, and Alois W. Schmalwieser. "Know your standard: clarifying the CIE erythema action spectrum." Photochemistry and photobiology 87, no.2 (2011): 483-486. for details. Considering that TEMIS uses the old (1987) norm, it is OK to use this norm throughout the paper, but the new norm could be mentioned.

We thank the reviewer for pointing us to the updated CIE spectrum. In the forthcoming upgrade of the TEMIS service, the updated CIE spectrum will be used: the expected impact on the UV index values will be small, but we consider that it is important to follow the official standard. We have rephrased the beginning of Sect. 2.2, where UVI-CIE is introduced.

"In the current v1.4 TEMIS service, the UVI is based on the CIE action spectrum described by McKinlay and Diffey (1987). Webb et al. (2011) describe an improved version of that action spectrum adopted by CIE in 1998. The effect of this improvement on the UVI values is small, well below 1% except for high solar zenith angle situations (Webb et al., 2011). The improved CIE erythemal action spectrum will be included in the forthcoming upgrade (v2.0) of the TEMIS service."

P4, L9: I note that the action spectrum for DNA damage suggested by Setlow (1974) is only defined for wavelengths up to 365 nm. The parameterization by Bernhard and Seckmeyer (1997), which was based on a suggestion by the NDSC steering committee (now NDACC), uses 370 as the terminal wavelength. In contrast, the spectrum drawn in Figure 1 goes up to 400 nm. The difference between the longest wavelength (365, 370, or 400 nm) is not negligible because additional contributions from the UV-A decrease the sensitivity to ozone considerably. The authors should ensure that the definition used by TEMIS is identical to that used in their work. Because the list of authors also includes colleagues that are involved in creating new versions of TEMIS products, I suggest that they carefully consider the latest definitions of the erythemal, DNA-damage, and Vitamin D action spectra when preparing a new TEMIS version.

We appreciate the comment. For this study we used the exact same action spectra with the ones that TEMIS uses to avoid discrepancies due to different applied spectra as you indicate.

P4, L13: Please specify the wavelength shift!
We now provide this information as stated bellow:
"The difference, which includes a wavelength shift of 3 nm (the applied action spectrum peaks at 295 nm and not at 298 nm as proposed by CIE), …"

P5, L6: No. Equation (1) already defines the UV Index. So either delete this sentence or define Eq. (1) and the subsequent descriptions at erythemally weighted irradiance.

In the TEMIS processing the UVI(t) is computed in W/m2 as indicated in Eq. (1), with a time dependent SZA(t), and as such it is used in the integration over time t to determine the daily UVD. Only when reporting the UV index at local solar noon UVI(t=12h) the scaling to dimensionless units is performed, which is why this sentence is present. Describing UVI(t) in Eq.(1) as "erythemally weighted irradiance" is a good idea, thank you – the idea has been implemented, but without "erythemally", as it is valid for all action spectra.

In the following sentence, UVD should be calculated by integrating the erythemally weighted irradiance instead of integrating the UVI.

Yes, the UVD is an integration over UVI(t) over time t from sunrise to sunset, with SZA(t) dependent on time, where UVI(t) is the UV index at time t. It sounds a little confusing perhaps, but calling the UV index at local solar noon (the quantity communicated to the public) just "UV index" is actually the confusing part of this.

We rephrased the whole description trying to convey this message.

P5, L9: If a cloud fraction within a 0.5◦x 0.5◦ grid cell is defined, the resolution of the satellite must be much better than 0.5◦x 0.5◦. What is it?

The cloud fraction is derived from the MSG cloud mask. The resolution of the MSG measurements varies with latitude/longitude: along longitude 0 the resolution at latitude 30N is about 0.04 degrees, and at latitude 60N it is about 0.08 degrees.

Eq. (4) is curious. If Ag is zero, fA should be 1. Yet it is 0.9775. When Ag is 1 (e.g., pristine new snow), it should be about 1.5 for erythemally weighted irradiance, yet it is only 1.3. Because Eq. (4) is part of the TEMIS code, it cannot be changed, however, it should be pointed out that the equation (which was empirically derived from measurements at two urban sites) may not be a good parameterization for large parts of the area relevant to the TEMIS UV product, which includes Scandinavia.

Eq. (4) is correct because it is emperically based on the (average) ground albedo Ag of the measurement sites used for the parameterization. This means that the albedo correction factor fA equals 1 for Ag=0.09.

Many factors determine the actual enhancement of the UV due to upward diffused radiation backscattered to the surface. We do not see why this should lead to a factor equal to 1.5.

P6, L25: "are less than 5.6%". Delete "less than". (The concept of "uncertainty" defines

a distribution (typically normal) and 5.6% defines the width of that distribution.)

We deleted it.

L6, L33: According to the text, only UVB-1 data were corrected for the degradation of the instrument's absolute spectral response. According to my knowledge, also NILU-UV instruments are subject to drifts. If the NILU-UV channels have drifted, as I suspect, a paragraph should be included in the manuscript describing how these drifts were corrected. How often was their calibration adjusted based on comparison with the Brewer? When comparing with the Brewer, did you take into consideration that the time associated with the Brewer measurements is different for every wavelength and did you interpolate NILU-UV measurements to the times of Brewer measurements?

Thank you for the comment. On the same page, line 26 we mentioned that NILU103 measurements were calibrated with coincident B086 measured irradiances.
We also added a paragraph, as suggested, to make sure that all the details are conveyed through the manuscript:
"Specifically, for the calibration of NILU103 raw data, cloud free response weighted irradiances were derived from B086's measured spectra. Since B086 scans the UV solar spectrum within approximately 7 minutes, the time period needed to scan the spectral range of each NILU103's channel spectral response, is approximately 3 minutes. The coincidences of NILU103's raw data to B086's weighted spectra, were performed based on the time that B086 measured the wavelength at which each channel peaks. Subsequently, the time difference that can be introduced between the two datasets is normally less than ±1 minute. To account for this time window, the mean values of 3 consecutive NILU103 measurements were analyzed, with the central one chosen to be the closest to B086's time scan of the peak wavelength of each channel. Then, NILU103's data were corrected for possible drifts in time via a time dependent smoothing spline fit. Furthermore, the drifts of the channels were monitored through monthly lamp measurements. Both methods resulted in the same patterns for the drifted channels.
After correcting for time drifts, a time independent absolute calibration factor is derived through scatter plots based on linear regression through origin. To evaluate the validity of the calibration procedures, the NILU103 calibrated data were compared once again with B086 response weighted irradiances and the timeseries were checked for time drifts and SZA dependence. By calibrating the NILU103 measurements with the B086 coincident response weighted irradiances, we estimate that the uncertainties of the NILU103 measurements used in this study are 5.6% (Zempila et a., 2016a)."

Section 3.2.1: Follow-up to the previous comment: what was the time associated with a effective doses calculated from the Brewer measurements? Since a Brewer spectrum takes several minutes to record, the time is ambiguous.

For the Brewer's effective doses, we considered as measuring time, the time when brewer scanned the wavelength of the peak for each action spectrum. For the DNA damage dose the starting time of the scan was taken into account. Since we used only cloud free cases, we consider that this approach doesn't introduce uncertainties larger than those of the NILU measurements themselves, even for larger SZAs.

The text was updated accordingly (page 7, lines: 27-31).

"The corresponding effective doses have been calculated by integrating the weighted spectra over the nominal wavelength range, while the time of measured doses was matched to the time that B086 scanned the wavelength where the highest sensitivity of each action spectrum is found. Since DNA damage action spectrum peaks at the lower measured wavelengths, the correspondent time was chosen to be the starting point of the scan. It appears that in most cases the 3 doses have time differences less than 1 minute."

Figure 2: Replace "mu" in legend with "Average"

Thank you. We have changed the first sentence in the caption from: "Model selection. (Top) The z-scores of the input variables and the erythemal UV dose (CIE)."

to:

"Model selection. (Top) Boxplots of the z-scores of the input variables and the erythemal UV dose (CIE) with mean values denoted by μ."

P9, L3: What is the variable "n"?. Line 12 suggests that n is the total number of data records. However, if log(n)ˆ1.5 = 36, n would be about 8E10 or 80 billion. This number must greatly exceed the number of NILU-UV data records!

n = 47,908 is the number of co-located input-output vectors (Page 8, Line 15). To help the reader, we have put log(n) inside brackets so that the expression now reads → (log(n))^1.5. Precisely, this gives 35.3793 which we rounded to the next multiple of 2 to get the value of 36 quoted in the manuscript (page 8, line: 27).

First paragraph Section 3.2.3: The description of the calculation of effective Vitamin D dose could be improved. For example: (1) Calculate effective dose for the response function of the UVB-1 (2) Convert this instrument response function weighted dose to erythemal dose taking into account SZA and total ozone (e.g., as described on page 6, line 29). (3) Convert erythemal dose to Vitamin D dose using the parameterization suggested by Fioletov et al. (2009). (4) Apply correction (Eq. (5)).

Thank you, we enriched this section.

P11, L9: The empirical relationship for DNA-damage effective dose is indeed very complex. What was the idea behind this complicated parameterization?

The initial idea was to get the DNA-damage effective dose from the CIE and the main factors that determine its levels, i.e. the TOC and the SZA in a relatively simple way (without involving look-up tables). Although the specific quantity could be directly derived from the Brewer spectra, getting it from the YES UVB-1 radiometer provides higher temporal resolution and more accurate calculation of the daily doses. We could not find a simpler parameterization than the one provided in the paper, for which the calculated quantities are accurate and unbiased from the dependent variables (TOC, SZA). Thus, although the parameterization is very complex we used it for the purposes of the present study. We provide it in the document since it might either be directly used by other people, or help them to find an improved, more general parameterization.

Eq. (6): In the second term, replace UVI with CIE.

Thank you, we did.

Eq. (8): The term CIEˆ3 appears twice, with coefficient a4 and with coefficient a6. This makes little sense. CIEˆ3 should only appear one with the coefficient a4+a6= -0.0354.

Thank you. It was a typo. The equation has been corrected properly.

P13, L10: Delete "exact"

Thank you, we did.

Figure 5: The seasonal variation in 2011 appears to be much stronger than in other years. What is the reason? Wildfires? Perhaps there is something interesting that could be learned!

The reviewer is correct. In early summer 2011, wildfires took place at the suburbs of the city, while data logging of the NILU's data was interrupted due to power failures resulting in less data points.

P15, L10 "...respectively." > "...respectively (Figure 7)."

Thank you, we did.

P17, L7 and Figure 8: The right side of Figure 8 only shows 5 discontinuities. I would expect many more if cloud information is updated every half hour, as the text indicates.

We think that discontinuities should be seen when the cloud information changes "significantly" within the 30 minutes steps. Based on the cloud information update frequency, a set of 3 points onto the graph corresponds to data with the same cloud information. If the cloud information does not change or changes slightly, discontinuities are absent of hard to be seen. Please check the changing point at around 800 (minutes) on the right hand plot of figure 8. We expect the changes to be seen within days with rapidly changing cloudiness conditions.

P17, L13: How were cloud-free data characterized? What dataset was used to determine sky condition?

The filter we are using for defining the cloud free cases stated on page 13, line 22 is the same for all comparisons, apart from figure 9 were we evaluate the cloud influence on the TEMIS-NILU comparisons. We added the following sentence in order to clarify this selection criterion (Page 13, lines: 23-25)

"This cloud classification criterion according to which days with more than 70% abundance of cloud free measurements are characterized as cloud free, is used throughout the study, unless stated otherwise."

Again on page 17, lines: 10-11, we also emphasize on this detail.

"At this point it should be mentioned that for the characterization of the cloud free one-minute data, the cloud screening detector proposed by Zempila et al. (2016a) was applied on the NILU103 Photosynthetically Active Radiation (PAR) measurements"

P19, L8 and Figure 10, and P22, L6: I don't see much difference in the slope for AOD < 0.4 and > 0.4. Perhaps the difference would become more obvious if the symbol size in Figure 10 were to be reduced.

Unfortunately resizing the marker size ends to a faint and hard to read figure. To support this statement, the linear fits of each dataset were calculated, one for <u>AOD<=0.4</u> and one for <u>AOD>0.4</u>. For all three daily doses, CIE, DNA damage and vitamin D, the slopes are significantly larger for AOD<=0.4 than those calculated for the cases where AOD was higher than 0.4. An additional paragraph provides this information into the text (page 20, lines: 5-9).

"To further testify on this aspect, linear fits were conducted for two datasets, one that comprised data with AOD≤0.4 and the second with data with corresponding AOD>0.4. It was found that for all three UV effective doses, the slopes for the first imposed limitation on AOD were higher than those calculated for the second dataset. Specifically, the slopes for the two AOD limitations were found to be 44.5% and 11.7% for the CIE, 50.6% and 8.5% for the DNA damage, 46.1% and 8.3% for the vitamin D doses respectively."

<u>**Appendix A**</u>**:**

Please specify the numbers of s1 and s2 (or the range if the numbers are not constant).

Thank you. We have explicitly stated the values of s1 and s2 in the appropriate sentence in the Appendix (Page 23, Lines 17-18) as follows:

“Layer 1 (the “hidden” layer) contains s1 = 13 neurons each having a nonlinear activation function f1 = tanh and Layer 2 (the “output" layer) contains s2 = 3 neurons each having a linear activation function f2.”

Technical corrections:

While the quality of the language is generally good, many sentences are too long and this affects the readability. Whenever possible and appropriate, the authors should reduce the length of sentences and split them in two.

We agree with the reviewer, thus, we shortened the sentences where possible.

P2, L5: Change “UV sunlight” to “solar radiation in the UV range”. By definition, “light” should only be used to describe wavelengths visible to the human eye.

Thank you for the information. It was changed to solar UV radiation.

P2, L6: Delete “extreme”. Mutations can technically be triggered by only one photon.

Thank you, we did.

P3, L5: “...product services started in the 2003 and...”

Thank you, we did change the sentence accordingly.

P3, L13: “following for example changes in the operationally assimilated...2003) which were initially based on the....and later on GOME-2...”

Thank you, we did change the sentence accordingly.

P3, L20: “... SEVIRI instruments that have been operational...”

Thank you, we did change the sentence accordingly.

P3, L32: “The UVI-CIE is given as a dimensionless number...”

Thank you, we did change the “UVI-CIE” to “UVI” in order to be consistent.

P4, L16: 'bare'? Finding a better word is indeed challenging. Perhaps: raw, uncorrected, approximate, first-guess...

We changed this to "first guess of the UV index".

P4, L17: "... is then calculated from UVI' by..."

Thank you, we did change the sentence accordingly.

P6, L10: "...triangular-like slit resulting in a bandwidth of 0.55 nm FWHM.

Thank you, we did change the sentence accordingly.

L6, L13: higher SZA > larger SZA (so not to confuse with "higher Sun")

Thank you, we did change the sentence accordingly.

P9, L21 and figure 3: I don't see any change in the colors of between a training fraction of 50% and 90%, consistent with the text. So if the proportion of training data has almost no effect, why is it so important to discuss this and include a figure? Is your point to illustrate that that your results are basically independent of t/n? The left figure could be simplified by plotting MSE versus the number of neurons.

Thank you, you are correct. As we describe in the text on Page 10, Lines 6-7, and as you note, the training MSE is not sensitive to the training fraction for large numbers of input-output vectors – rather it is sensitive to the number of neurons. While we agree that the same conclusion can be drawn by plotting MSE versus neurons, there would be a loss of information on the lack of sensitivity to training fraction. The left figure embraces both concepts in one go and is why we decided against doing this.

P9, L33: "ballpark" > "rough" or "approximate"

Thank you, we did change that to rough.

P15, L10: datasets are > datasets is

Thank you, we changed all occurrences.

P18, L7: either of the > all

Thank you, we changed this point.

P18, L11: Move "on average" to end of sentence.

Thank you, we changed this point.

P19, L24: "in the" > of

Thank you, we changed this point.

P21, L25: moments > periods

Thank you, we changed this point.

P21, L28: "limits the dataset by almost 75%" > "make up only 25% of the dataset" (if that's what you want to say)

Changed to "The number of cloud-free days limits the dataset to one fourth of the original, while …"

<u>Reviewer #2: Comments and Suggestions</u>

1. All-skies and clear-skies in figs 5, 6, 9: The scatter plots in figs 5 and 6 for the case of all-skies are very different. Monthly variations and standard deviations are also very different. In fig. 5 I also note that the all-skies vs clear-skies scatter plots, and associated monthly variations and standard deviations, agree very well, something that is not seen in fig. 9. I understand that the UVB-1 and NILU data have been calibrated to a Brewer instrument before use, while the TEMIS data have not. Given that the Brewer favours measurements when the sun is not covered by clouds, can it be that this pre-calibration affects the measurements so that the all-skies in fig. 5 are not actually all-skies as in figs 6 and 9 but semi all-skies? Also, what filter do you use to define the clear-skies in fig. 5? Moreover, given that fig. 5 compares UVB-1 vs NILU data both calibrated to the same Brewer, while figs 6 and 9 compares TEMIS vs NILU data (NILU pre-calibrated to Brewer, TEMIS being not), would it make sense to calibrate also the TEMIS data to the Brewer for consistency? Potentially this pre- calibration reduces part of the variance in the original UVB-1 and NILU data, and as a consequence a better comparison is achieved between the two radiometers. I am not sure. Have you checked if the calibration to the Brewer affects the measurements denoted as all-skies? Overall I think that a clarification on the definition of all-skies and clear-skies conditions would help the reader.

Thank you for this comment. Here, we should notice that the UVB-1 data were not calibrated against the Brewer, but were only monitored and partially corrected for random incidences and occasional drifts caused by logging and/or electronic issues we have been experiencing during some short periods. Our intention was to prove that the NN originally applied to the NILU irradiances, results in reliable data firstly for CIE estimations, and secondly for vitamin D and DNA damage doses. We are aware that the UVB-1 data are not cosine corrected while a small overestimation of CIE takes place during the summer months. This behavior could explain the small seasonality seen in the two CIE datasets, UVB-1 and NILU (Figure 5(a)). We hope that the statement on page 13, lines: 14-16 adequately explains these aspects:
"Even though the UVB-1 data were corrected for the degradation of its absolute response with B086 data, the validity of its measurements as absolute values can be used to evaluate the performance of the NN used to derive all of the biological dose products based on NILU-UV measurements."

For the NILU calibration, you are correct, we used only cloud free cases to derive the final irradiances. A detailed explanation of the NILU calibration procedures was added to the text. "Specifically, for the calibration of NILU103 raw data, cloud free response weighted irradiances were derived from B086's measured spectra. Since B086 scans the UV solar spectrum within approximately 7 minutes, the time period needed to scan the spectral range of each NILU103's channel spectral response, is approximately 3 minutes. The coincidences of NILU103's raw data to B086's weighted spectra, were performed based on the time that B086 measured the wavelength at which each channel peaks. Subsequently, the time difference that can be introduced between the two datasets is normally less than ±1 minute. To account for this time window, the mean values of 3 consecutive NILU103 measurements were analyzed, with the central one chosen to be the closest

to B086's time scan of the peak wavelength of each channel. Then, NILU103's data were corrected for possible drifts in time via a time dependent smoothing spline fit. Furthermore, the drifts of the channels were monitored through monthly lamp measurements. Both methods resulted in the same patterns for the drifted channels.
After correcting for time drifts, a time independent absolute calibration factor is derived through scatter plots based on linear regression through origin. To evaluate the validity of the calibration procedures, the NILU103 calibrated data were compared once again with B086 response weighted irradiances and the timeseries were checked for time drifts and SZA dependence. By calibrating the NILU103 measurements with the B086 coincident response weighted irradiances, we estimate that the uncertainties of the NILU103 measurements used in this study are 5.6% (Zempila et a., 2016a)."
Based on these given details, NILU are considered to be valid for all skies cases and Brewer measurements do not affect the all skies measurements by means of implicitly excluding them. This is further testified by the fact that the agreement between UVB-1 and NILU derived CIE lies within the uncertainty of the latter, even for overcast days.
Following your sequence of thoughts, we believe that now it is more clear that UVB-1 and NILU CIE data are independent when compared in absolute values, since Brewer data served only for occasional drift correction in the UVB-1 while they were used for time drifts and absolute calibration of NILU raw data. We also agree that a pre-calibration of the TEMIS products based on Brewer measurements could take place, but the scope of this paper is to compare independent sources of estimations derived from satellite- and ground-based instruments, in our case NILU and TEMIS, in order to identify possible reasons of discrepancies between the two datasets. The comparisons performed for UVB-1 and NILU were meant to only evaluate the NN retrieval algorithm.

The filter we are using for defining the cloud free cases stated on page 13, line 22 is the same for all comparisons, apart from figure 9 were we evaluate the cloud influence on the TEMIS-NILU comparisons. We added the following sentence in order to clarify this selection criterion (Page 13, lines: 23-25)
"This cloud classification criterion according to which days with more than 70% abundance of cloud free measurements are characterized as cloud free, is used throughout the study, unless stated otherwise."
Again on page 17, lines: 10-11, we also emphasize on this detail.

"At this point it should be mentioned that for the characterization of the cloud free one-minute data, the cloud screening detector proposed by Zempila et al. (2016a) was applied on the NILU103 Photosynthetically Active Radiation (PAR) measurements"

2. Page 19, line 2: The seasonality of the cloud-free cases is said to match the seasonality of all-skies but it is not shown. My suggestion is to show the seasonality of the cloud-free cases because later in fig. 10 you try to explain the cause of a seasonality which is not actually shown. The seasonality can be added in fig. 9 for the lines shown in fig. 9 accordingly. I expected that the seasonality of the cloud-free cases will match the seasonality of the clear-

skies shown in fig. 5 not of the all-skies shown in fig. 6. Cannot understand why since we are talking about cloud-free data. A match between the two clear-skies seasonalities would strengthen the findings about clouds affecting the TEMIS data.

We thank you for the suggestion. We added the seasonality of the TEMIS/NILU comparisons for the 4 cloud classifications in the lower panel of Figure 9. Based on the findings, we cannot say that the seasonality seen in Figure 5 is the same with the one seen for the cloud free cases (Ncl>70%) in Figure 9. Although one could say that there are some similarities, when comparing these two seasonality patterns a solid conclusion is hard to be driven. We believe that these patterns are surely connected to the NILU data, but we also believe that the seasonality seen in the UVB-1/NILU comparisons is mainly due to the missing cosine correction of the UVB-1 data. On the other hand, the seasonality seen with the TEMIS/NILU comparisons can be attributed to both cosine inadequate treatment in the NILU data and/or satellite data and to the nature of the a-priori information used in the TEMIS algorithm. The pertinent paragraph was modified accordingly:

"Table 3 shows that even under cloud-free days there is a scatter of almost ±13% between the two datasets for all three UV doses. The seasonality seen in Figure 6 is also present when limiting the datasets to cloud-free days, as seen in the lower panel of Figure 10, implying that apart from the cloud effects, there are other factors affecting the agreement between the ground- and satellite-based UV data products. One of the causes could be variability of aerosol load over Thessaloniki which is neglected in the satellite-based retrievals."

3. Aerosol effect, p. 19 and fig 10: It is claimed that one of the causes for the seasonality seen in the satellite minus ground-based clear-sky differences (which is not actually shown) is variability in the aerosol load. The authors use fig. 10 to support this. Fig. 10 shows that there is a relation between the satellite minus ground-based clear-sky differences with increasing AOD (using 10-minute time intervals), revealing a positive correlation between them, but it does not straightforwardly show the link between their seasonal variations. What is the shape of the two seasonalities and how do they match? I suggest adding an extra plot in fig. 10 (below the existing plot) showingexplicitly the monthly variation of the differences vs the monthly variation of aerosols. This would strengthen the claim on p.19 line 4.

We again thank you for the suggestion. We added the seasonalities of all datasets shown in Figure 10 for the cloud free 10-minute doses. A description was also added into the text to further analyze the findings.

"To further investigate the AOD impact on the comparisons, the monthly means were calculated for both AOD and relative differences. The pattern seen in the monthly means of the AOD values is in general agreement with the seasonality seen in the average monthly values of the relative percentage differences between the satellite- and ground-based 10-minute cloudless doses (Figure 10, lower panel), implying that there is a link between the two observed seasonalities."

4. Page 19, lines 8-12: According to section 2.2 (p.5 lines 29-30), for AOD>0.3 the satellite UV data products will overestimate the UV index and UV dose. Indeed, the negative differences

in fig. 10 tend to become positive for AOD>0.3 (indicating the satellite overestimation), but it is not clear what you mean by mentioning that the slope changes for AOD>0.4. Do you imply that there is better agreement between the satellite and ground-based data in larger AOD? I think that mentioning about two slopes confuses, unless if you clarify what you mean.

To support this statement, the linear fits of each dataset were calculated, one for AOD<=0.4 and one for AOD>0.4. For all three daily doses, CIE, DNA damage and vitamin D, the slopes are significantly larger for AOD<=0.4 than those calculated for the cases where AOD was higher than 0.4. An additional paragraph provides this information into the text (page 20, lines:1-5).

"To further testify on this aspect, linear fits were conducted for two datasets, one that comprised data with AOD≤0.4 and the second with data with corresponding AOD>0.4. It was found that for all three UV effective doses, the slopes for the first imposed limitation on AOD were higher than those calculated for the second dataset. Specifically, the slopes for the two AOD limitations were found to be 44.5% and 11.7% for the CIE, 50.6% and 8.5% for the DNA damage, 46.1% and 8.3% for the vitamin D doses respectively."

5. Is there relation between the seasonality in aerosols and the seasonality in the UVB-1 minus NILU clear-sky differences?

To further investigate this aspect, we used the cloud free cases for both TEMIS/NILU and UVB- 1/NILU comparison results. As seen in the figure bellow, it seems that there isn't any strong correlation between the seasonality of AOD and (UVB1-NILU)/NILU% data.

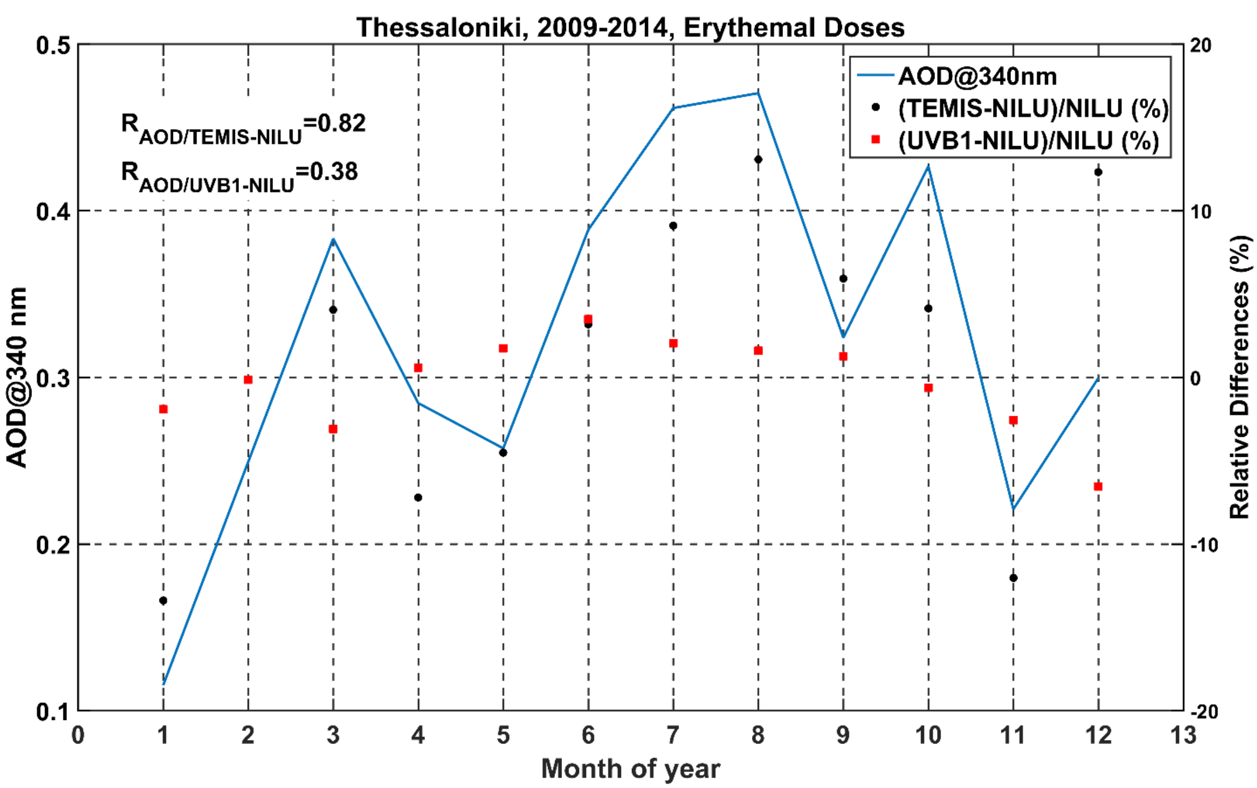

<u>Minor comments:</u>

Eq. 1: remove the unit (W/m2) from the UV index.

In the TEMIS processing the UVI(t) is computed in W/m2 with a time dependent SZA. As such it is used in the integration over time t to determine the daily UVD. Only when reporting the UV index at local solar noon UVI(t=12h) the scaling to dimensionless units is performed, as mentioned in the sentence at page 5 / line 6 (old numbering). Hence, we leave the unit in Eq. (1); the sentence at p5/l6 has been adapted slightly.

Page 5, lines 6-8: Is it correct that the daily UV dose is calculated from the UV index?

Yes, the UVD is an integration over UVI(t) over time t from sunrise to sunset, with SZA(t) dependent on time, where UVI(t) is the UV index at time t. It sounds a little confusing perhaps, but calling the UV index at local solar noon (the quantity communicated to the public) just "UV index" is actually the confusing part of this.

Page 6, line 30: It reads '...the total ozone column (TOC) and are used...'. Is it something missing from the sentence?

Thank you, we rephrased that to "…the total ozone column (TOC). These factors are used to…".

Page 10, line 3: correct 'NILY' to 'NILU'.

Thank you, we did.

Page 15, line 9: Usually the correlation values are usually re given by the correlation coefficient R, not the Rˆ2.

We thank you for the comment. R values were added to tables 3 and 4, while additional comments on these values were included in the text along with the discussion regarding the R^2 values.

Page 18, line 5: correct 'bellow' to 'below'.

Thank you, we did.

Fig. 5: Please put (a), (b) and (c) to the left side of the titles of the plots, not below the plots.

Thank you, we did.

Fig 6: Indicate that the figure refers to all skies.

Thank you, we did.

Fig. 7: Indicate that the figure refers to all skies. Use thicker lines for the linear lines, and use dots or dashes for the y=x line.

Thank you, we did.

Fig. 10: remove the three ‘y=’ inside the legend since these statistics are not equations. Also, indicate that the figure refers to the >90% cloudless instances, if so.

Thank you, we revised the legend and changed the caption to:

“Relative differences of satellite-based and ground-based UV 10-minute doses as a function of AOD at 340 nm for cloudless cases at Thessaloniki in the period 2011-2014. The statistics are provided in the form of mean and standard deviation of the differences (upper panel). Monthly mean values of AOD at 340 nm along with the mean monthly values of the relative differences presented in the upper panel under cloud free cases (lower panel).”

TEMIS UV product validation using NILU-UV ground-based measurements in Thessaloniki, Greece

Melina-Maria Zempila[1*,2], Jos H. G. M. van Geffen[3], Michael Taylor[2], Ilias Fountoulakis[2], Maria-Elissavet Koukouli[2], Michiel van Weele[3], Ronald J. van der A[3], Alkiviadis Bais[2], Charikleia Meleti[2], and Dimitrios Balis[2]

[1]USDA UV-B Monitoring and Research Program, Colorado State University, Fort Collins, Colorado 80523, U.S.A.
[2]Laboratory of Atmospheric Physics, Aristotle University of Thessaloniki, PO Box 149, 54124, Thessaloniki, Greece.
[3]Royal Netherlands Meteorological Institute (KNMI), De Bilt, The Netherlands.

Correspondence to: Melina Maria Zempila (melina.zempila@colostate.edu)

Abstract. This study aims to cross-validate ground-based and satellite-based models of three photobiological UV effective dose products: the CIE erythemal UV, the production of vitamin D in the skin and DNA-damage, using high temporal resolution surface-based measurements of solar UV spectral irradiances from a synergy of instruments and models. The satellite-based Tropospheric Emission Monitoring Internet Service (TEMIS; version 1.4) UV daily dose data products were evaluated over the period 2009 to 2014 with ground-based data from a NILU-UV multifilter radiometer located at the Northern mid-latitude super site of the Laboratory of Atmospheric Physics, Aristotle University of Thessaloniki (LAP/AUTh) in Greece.

For the NILU-UV effective dose rates retrieval algorithm, a neural network (NN) was trained to learn the nonlinear functional relation between NILU-UV irradiances and collocated Brewer-based photobiological effective dose products. Then the algorithm was subjected to sensitivity analysis and validation. The correlation of the NN estimates with target outputs was high (r=0.988 to 0.990) and with a very low bias (0.000 to 0.011 in absolute units) proving the robustness of the NN algorithm. For further evaluation of the NILU NN derived products, retrievals of the vitamin D and DNA-damage effective doses from a collocated YES UVB-1 pyranometer where used. For cloud free days, differences in the derived UV doses are better than 2% for all UV doses products, revealing the reference quality of the ground-based UV doses at Thessaloniki from the NILU-UV NN retrievals.

The TEMIS UV doses used in this study, are derived from ozone measurements by the SCIAMACHY/Envisat and GOME2/MetOp-A satellite instruments, over the European domain in combination with SEVIRI/Meteosat based diurnal cycle of the cloud cover fraction per $0.5^\circ \times 0.5^\circ$ ($lat \times lon$) grid cells. TEMIS UV doses were found to be $\sim$12.5% higher than the NILU NN estimates but, despite the presence of a visually apparent seasonal pattern, the R^2 values were found to be robustly high and equal to 0.92-0.93 for 1,588 all sky coincidences. These results significantly improve when limiting the dataset to cloud free days with differences of 0.57% for the erythemal doses, 1.22% for the vitamin D doses and 1.18% for the DNA-damage doses, with standard deviations of the order of 11-13%. The improvement of the comparative statistics under cloud-free cases further testifies to the importance of the appropriate consideration of the contribution of clouds in the UV radiation reaching the Earth's surface. For the urban area of Thessaloniki with highly variable aerosol the weakness of the implicit aerosol information introduced to the TEMIS UV dose algorithm was revealed by comparison of the datasets to aerosol optical depths

at 340 nm as reported by a collocated CIMEL sunphotometer, operating in Thessaloniki at LAP/AUTh as part of the NASA Aerosol Robotic Network.

1 Introduction

During the last few decades, the danger of overexposure to ~~UV sunlight~~ solar UV radiation has been well analysed and a causal link has been established to skin diseases and cancer since the mutation of DNA can be triggered by ~~extreme~~ UV-B doses (Xiang et al., 2014; Parkin et al., 2011; Berwick et al., 2005; Setlow, 1974, among others). ~~Furthermore~~On the other hand, the cutaneous production of vitamin D~~is~~, a ‘vitamin’ that is proven to be essential for human health, is also activated by spectral UV radiation~~, hence~~. Hence accurate knowledge of ‘safe’ UV doses for humans is paramount in order to balance the harmful and beneficial effects of UV exposure (McKenzie et al., 2009; Webb et al., 1988; MacLaughlin et al., 1982, among others). Of particular relevance is the Commission Internationale de l’ Éclairage (CIE) action spectrum as a model for the susceptibility of skin to sunburn (erythema) (McKinlay and Diffey, 1987). As a result of advances in the fields of photobiology and ground-based measurements of UV using different types of instrumentation, a variety of methods now exist to obtain erythemal, vitamin D and DNA-damage dose rates (Kazantzidis et al., 2009; Webb and Engelsen, 2006; Pope et al., 2008; Engelsen et al., 2005; Samanek et al., 2006).

In parallel, space technology has been making huge steps forward to monitor the Earth 's surface and atmosphere at higher spatial and temporal resolution and erythemal, vitamin D and DNA-damage dose rates and doses can now be retrieved globally from solar backscattered radiation observations from different satellite sensors. Subsequently, long, reliable and high temporal resolution ground-based estimates of surface photobiological effective dose quantities are of high importance in order to validate and characterize the satellite-derived UV products. Ozone layer depletion and recovery in times of climate change reinforce the need for establishing global long-term and quality assured climate data records of the incident solar UV daily doses at the surface.

In this study, photobiological UV daily doses retrieved from ground-based measurements using empirical models and satellite estimates are cross-validated to assess their accuracy and potential utility.

2 TEMIS satellite-based UV data products

2.1 Operational services

The Tropospheric Emission Monitoring Internet Service (TEMIS) was established in 2001 at the Royal Netherlands Meteorological Institute (KNMI) as part of a project from the European Space Agency (ESA) and the service has been maintained since. The TEMIS UV data product services ~~,~~started in 2003 ~~,~~and are available through the webportal at http://www.temis.nl/uvradiation/. The UV products, currently version 1.4, are produced in near-real time on alatitude $\times$ longitude grid of $0.5^\circ \times 0.5^\circ$ and consist of data sets, maps, and time series. The products are calculated using operational satellite data streams of the global ozone distribution and, over Europe, the diurnal variation in cloud cover fraction.

The TEMIS UV data products essentially exploit the empirically-based parametrisation by Allaart et al. (2004) of the amount of UV radiation incident at the surface in $\mathrm{W/m^2}$, as function of the total ozone column and the solar zenith angle at a given local solar time, taking into account an appropriate action spectrum, i.e. the wavelength dependent response to UV radiation of health effects or otherwise.

Since the initiation of the TEMIS UV services maintenance and updates were implemented following for example changes in the operational assimilated global ozone distribution (Eskes et al., 2003), which were based on the SCIAMACHY instrument aboard ENVISAT (Bovensmann et al., 1999) up to April 2012, and later on GOME-2 aboard MetOp-A (Hassinen et al., 2016). Recently, the global ozone Multi-Sensor Reanalysis version 2 (MSR-2) by van der A et al. (2015) has been used to create a reanalysis of the global clear-sky UV index for a longer historical period (from November 1978 to December 2012).

Cloud attenuation over Europe is prescribed using the near-real time cloud mask product (Derrien and Le Gléau, 2005) provided by the EUMETSAT Nowcasting Satellite Application Facility (NWC-SAF), which is received, processed and archived at KNMI since July 2005. The operational cloud cover data set has been based on the different SEVIRI instruments that have been operational aboard the Meteosat Second Generation (MSG) satellites from January 2004 onwards using the Meteosat 8, 9 and 10 platforms, respectively. The effect of grid cell average surface elevation, though not the actual 3-D topography, on surface UV is taken into account in the calculations. Changes in surface albedo are prescribed using a monthly climatology of surface reflectivity (Herman and Celarier, 1997). The effects of aerosols are included implicitly in the parameterization but do not vary over time (Badosa and van Weele, 2002).

2.2 Products and algorithms

TEMIS provides two types of surface UV products: (i) the clear-sky erythemal UV index and (ii) the daily UV dose (daily integral) related to different health effects. The erythemal UV index (~~UVI-CIE~~UVI) is determined using the action spectrum adopted by the International Commission on Illumination (CIE) for erythema or reddening of the skin due to sunburn~~(McKinlay and Diffey, 1987).~~. In the current v1.4 TEMIS service, the UVI is based on the CIE action spectrum described by McKinlay and Diffey (1987). Webb et al. (2011) describe an improved version of that action spectrum adopted by CIE in 1998. The effect of this improvement on the UVI values is small, well below 1% except for high solar zenith angle situations

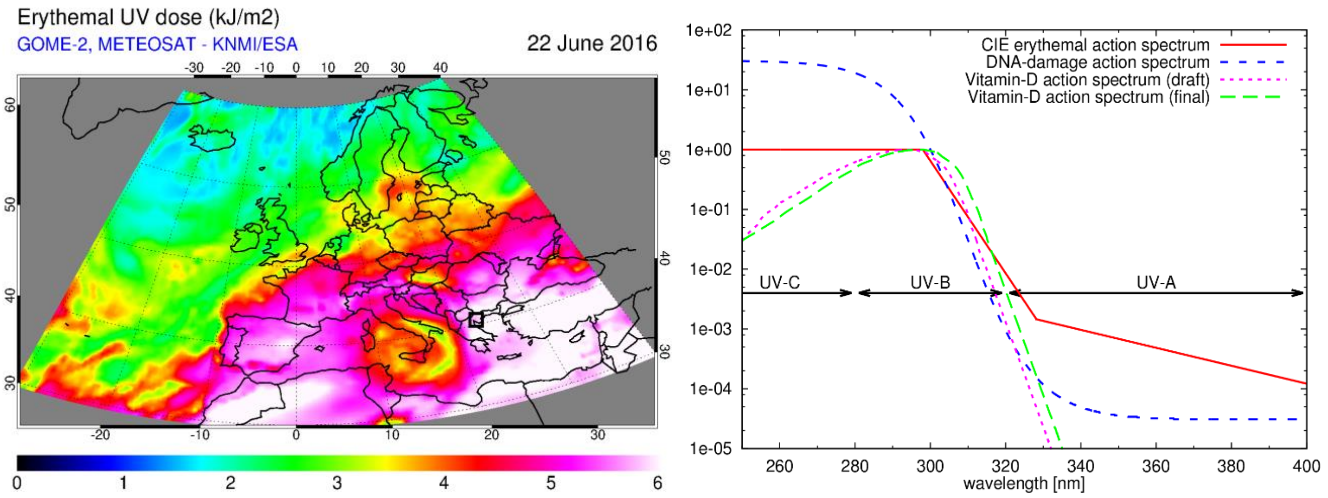

Figure 1. Erythemal UV dose over Europe on 22 June 2016. Thessaloniki, indicated by a black square, had an almost cloud-free day with an erythemal UV dose of 5.77 $\mathrm{kJ/m^2}$ and an erythemal UV index of 10.1 (left panel). Action spectra of erythema (red solid), generalized DNA-damage (blue short-dashed), and production of vitamin D (magenta dotted: draft version as used within TEMIS (Holick et al., 2005), and green long-dash: final version as adopted by the CIE (Bouillon et al., 2006) (right panel).

(Webb et al., 2011). The improved CIE erythemal action spectrum will be included in the forthcoming upgrade (v2.0) of the TEMIS service.

Following international agreements, the ~~UVI-CIE~~ UVI represents the amount of UV radiation at local solar noon, i.e. when the sun is highest in the sky, under clear-sky conditions. The ~~UVI-CIE~~ UVI is usually given as a dimensionless index, where 1 unit equals 25 $\mathrm{mW/m^2}$. Using the operational meteorological data streams (temperature, pressure, winds) which are included in the ozone data assimilation (Eskes et al., 2003), the ~~UVI-CIE~~ UVI is available in forecast mode and TEMIS provides forecasts of both the global ozone field and ~~UVI-CIE~~ UVI for today and the coming 8 days.

The daily UV dose (UVD) is the total amount of UV radiation, usually given in $\mathrm{kJ/m^2}$, integrated between sunrise and sunset, accounting for the variation in the solar zenith angle (SZA) and cloud cover fraction (in TEMIS ~~(~~version 1.4) this is available over Europe only) during the day, see Figure 1, left. The UV dose is calculated for three action spectra (see Figure 1, right) : the erythemal UV dose (UVD-CIE) based on the CIE erythemal action spectrum (McKinlay and Diffey, 1987), identical to the one used for the UVI-CIE; the generalised DNA-damage UV dose (UVD-DNA) based on the action spectrum determined by Setlow (1974) and normalised at 300 nm based on Bernhard and Seckmeyer (1997); the vitamin D UV dose (UVD-VitD) based on the action spectrum for the production of previtamin-D3 in the human skin (Holick et al., 2005).

Note that the 2005 (draft) version by Holick et al. (2005) used for UVD-VitD within TEMIS differs ~~slightly~~ from the CIE adopted vitamin D action spectrum (Bouillon et al., 2006), see Figure 1, right. The difference, which includes a wavelength shift of 3 nm (the applied action spectrum peaks at 295 nm and not at 298 nm as proposed by CIE), would increase the TEMIS data by a factor of about 2.2 (2.1 in summer, 2.3 in winter) when using the CIE vitamin D action spectrum - ~~a~~ an important change that will be implemented in a forthcoming update (v2.0) of the TEMIS UV operational data streams.

For each action spectrum, a parametrisation is applied following Allaart et al. (2004) for the UV solar irradiance as a function of SZA(t) and total ozone column, providing a ~~'bare' UV index~~ first guess of the UV irradiance weighted with a specific action spectrum (UVI$'$), at time t using the global assimilated ozone field at local solar noon ($t = 12\mathrm{h}$). The final UVI(t), which can be seen as the UV index at time ~~t is then found from UVI$'$ after~~ t (i.e. with a time dependent SZA), is then calculated from UVI'(t) by applying a set of correction factors:

$$\mathrm{UVI}(t) = \mathrm{UVI}'(t) \cdot f_D \cdot f_C \cdot f_H \cdot f_A \qquad [\mathrm{W/m^2}] \tag{1}$$

where f_D is the correction for the day-to-day variation in the Sun-Earth distance, f_C the correction for the attenuation due to clouds (in case of clear-sky conditions: $f_C = 1$), f_H the correction for the surface elevation, and f_A the correction for the ground albedo.~~At this point it should be mentioned that the~~

The UVI index at local solar noon, UVI ($t = 12\mathrm{h}$), follows directly from Eq. (1), i.e. using SZA ($t = 12\mathrm{h}$), after devision by 25 (mW/m^2). The TEMIS products' uncertainty can currently be estimated only from the errors reported in the ozone total amount, thus it ~~only~~ reflects the lower boundary of the errors seen in the UV doses. Based on this fact, TEMIS products include an uncertainty of 2-3% in the daily doses. ~~The UV index at local solar noon, UVI($t = 12\mathrm{h}$), follows directly from Eq. (1) after division by 25 .~~The UVD products, in $\mathrm{kJ/m^2}$, are determined from a 10-min step integration of UVI(t), with a time dependent SZA, over time t between sunrise and sunset, which are assumed to lie symmetrical around local solar noon.

For the calculation of f_C the NWC-SAF cloud mask is converted to a cloud fraction (C_f) by counting the clear vs. cloudy instances per UV grid cell of $0.5° \times 0.5°$ (latitude $\times$ longitude). The cloud correction factor in Eq. (1) is then given by:

$$f_C = \begin{cases} 1.0 & , \quad C_f < 0.02 \\ 0.9651 - 0.2555 \cdot C_f & , \quad 0.02 \leq C_f \leq 0.98 \\ 0.5 & , \quad C_f > 0.98 \end{cases} \tag{2}$$

a relationship that has been determined from the effect of clouds on surface UV at the location of KNMI at De Bilt in The Netherlands (van Geffen et al., 2004; van Weele et al., 2005). For the calculation of f_H a 5% increase of the incident UV irradiance per km surface elevation above sea level is assumed:

$$f_H = 1 + 0.05 \cdot H \tag{3}$$

where the surface elevation H (in km) is determined from the GTOPO30 database (https://lta.cr.usgs.gov/GTOPO30/), resampled to the $0.5° \times 0.5°$ UV grid. For the calculation of f_A the following function of ground albedo (A_g) is applied, taking into account multiple reflections between the surface and the overlying atmosphere:

$$f_A = \frac{1 - 0.25 \cdot 0.09}{1 - 0.25 \cdot A_g} \tag{4}$$

The function derives from the series $1 + xy + (xy)^2 + \cdots = 1/(1 - xy)$ where $x = 0.25$ is the UV albedo of the overlying atmosphere for upward reflected UV radiation and $y = A_g$. Since the Allaart et al. (2004) UV index ~~parametrisation is empiraly~~

parameterization is empirically based on UV data collected at De Bilt and Paramaribo, the A_g at these (urban) sites $-$ with a 12-month average value of 0.09 $-$ is used as a ~~normalisation~~ normalization factor for the calculation of f_A. The data for A_g at each UV grid cell are taken at 335 nm from the monthly TOMS/GOME climatology, which uses the spectral dependency of the GOME database (Koelemeijer et al., 2003) but with a scaling to match the TOMS 340/380 nm database (Herman and Celarier, 1997; Boersma et al., 2004).

Note that there is no explicit correction in Eq. (1) for the variable presence of aerosols in the TEMIS UV data products. However, the Allaart et al. (2004) empirically-based parametrization includes an implicit aerosol correction due to the average aerosol load over these two urban sites: an AOD at 368 nm of 0.3 and an aerosol single scattering albedo (SSA) of 0.9 (Badosa and van Weele, 2002). For situations where the real aerosol load is lower (higher) than that assumed load, the UV data products will underestimate (overestimate) the UV index and UV dose. With potential future near-real time availability of aerosol optical parameters at a global scale, the correction factors derived by Badosa and van Weele (2002) could be applied within future updates of the TEMIS UV services.

3 Ground-based data products

3.1 Instruments at Thessaloniki

The calculation of the photobiological doses over Thessaloniki (40.63°E, 22.96°N) are based on measurements taken by three different types of instruments in continuous operation at the Laboratory of Atmospheric Physics of the Aristotle University of Thessaloniki (LAP/AUTh: http://lap.physics.auth.gr).

Firstly, a Brewer MKIII spectrophotometer with serial number #086 (B086) is equipped with a double monochromator and measures the UV solar irradiance spectrum (286.5 - 363 nm) with a wavelength step of 0.5 nm~~within~~. Every scan lasts 7 minutes ~~using~~ while the use of a triangular-like slit ~~that has a~~ results in a bandwidth of 0.55 nm full width at half maximum (FWHM)~~of 0.55~~. The spectra used in this study have recently been subjected to quality control and re-evaluation (Fountoulakis et al., 2016a) after which the remaining 1-sigma uncertainty is estimated to be 5% (Garane et al., 2006) for wavelengths longer than 305 nm and for solar zenith angles (SZA) smaller than 80°. For lower wavelengths and ~~higher~~ larger SZA the uncertainty is larger as a consequence of the photon noise that dominates due to the low recorded signal (Fountoulakis et al., 2016b). The simpler, single monochromator Brewer with serial number #005 (B005) has been operational in Thessaloniki since 1982 and has been providing continuous, well-calibrated and documented total ozone column measurements (Bais et al., 1985; Meleti et al., 2012; Zerefos, 1984).

Secondly, a Norsk Institutt for Luftforskning (NILU)-UV multi-filter radiometer has been fully operational in Thessaloniki since 2005 and forms part of the UVNET network of NILU-UV radiometers (http://www.uvnet.gr, Kazantzidis et al. (2006)). The NILU-UV with serial number 04103 (NILU103) provides one-minute measurements in 5 UV channels with nominal central wavelength at 302, 312, 320, 340 and 380 nm and a FWHM of 10 nm; while its sixth channel measures the Photosynthetically Active Radiation (PAR), and is used here to determine cloud-free cases based on the cloud detection algorithm proposed by Zempila et al. (2016a). Although the B086 measures the UV spectrum with high spectral resolution, the time frequency of the scans usually varies from 20 to 40 minutes. Nevertheless, Brewer spectrophotometers are a very powerful means for calibrating other UV measuring instruments that provide higher temporal resolution measurements.

Specifically, for the calibration of NILU103 raw data, cloud free response weighted irradiances were derived from B086's measured spectra. Since B086 scans the UV solar spectrum within approximately 7 minutes, the time period needed to scan the spectral range of each NILU103's channel spectral response, is approximately 3 minutes. The coincidences of NILU103's raw data to B086's weighted spectra, were performed based on the time that B086 measured the wavelength at which each channel peaks. Subsequently, the time difference that can be introduced between the two datasets is normally less than ± 1 minute. To account for this time window, the mean values of 3 consecutive NILU103 measurements were analyzed, with the central one chosen to be the closest to B086's time scan of the peak wavelength of each channel. Then, NILU103's data were corrected for possible drifts in time via a time dependent smoothing spline fit. Furthermore, the drifts of the channels were monitored through monthly lamp measurements. Both methods resulted in the same patterns for the drifted channels. After correcting for time drifts, a time independent absolute calibration factor was derived through scatter plots based on linear regression through origin. To evaluate the validity of the calibration procedures, the NILU103 calibrated data were compared once again with B086 response weighted irradiances and the timeseries were checked for time drifts and SZA dependence. By calibrating the NILU103 measurements with the B086 coincident response weighted irradiances, we estimate that the uncertainties of the NILU103 ~~irradiance~~ measurements used in this study are ~~less than~~ 5.6% (Zempila et al., 2016b).

Thirdly, a Yankee Environmental System (YES) UVB-1 radiometer operating also in Thessaloniki, provides one minute erythemal dose measurements with a spectral response very similar to the erythemal action spectrum (McKinlay and Diffey, 1987). Using model simulations with the libRadtran radiative transfer (Emde et al., 2016) proper weighting factors are calculated with respect to SZA and the total ozone column (TOC)~~and~~. These factors are used to transform the UVB-1 measurements into erythemal irradiance (Lantz et al., 1999). A similar transformation is applied for the Vitamin D and DNA-damage weighted irradiances (see section 3.2.3). In addition, the Brewer measurements have been used to correct the UVB-1 observations for the degradation of its absolute spectral response and for sudden changes in the behaviour of the instrument. Thus, the datasets from the UVB-1 and the NILU-UV radiometers are not completely independent since the Brewer instrument was used for the calibration of both instruments.

In addition, at Thessaloniki, a CE318-N Sun Sky photometer, also known as CIMEL, provides continuously atmospheric observations through the NASA Aerosol Robotic Network (AERONET) (Balis et al., 2010). CIMEL is providing aerosol optical depth at the UV wavelength of 340 nm, amongst other aerosol properties, which is used to investigate the effects of aerosol variability at Thessaloniki on comparisons with the satellite-derived UV products.

3.2 Products and Algorithms

3.2.1 Effective UV doses from the Brewer spectrophotometer

The B086 spectra were processed by the SHICrivm algorithm and extended to 400 nm (Slaper et al., 1995). The extended spectra were validated with a collocated EKO UV-A instrument (Zempila et al., 2016b) and weighted with the action spectra for: i) the erythemal dose (McKinlay and Diffey, 1987), ii) the formation of vitamin D in the human skin (Holick et al., 2005), and iii) DNA-damage (Setlow, 1974). The corresponding effective doses have been calculated by integrating the weighted spectra over the nominal wavelength range, while the time of measured doses was matched to the time that B086 scanned the wavelength where the highest sensitivity of each action spectrum is found. Since DNA damage action spectrum peaks at the lower measured wavelengths, the correspondent time was chosen to be the starting point of the scan. It appears that in most cases the 3 doses have time differences less than 1 minute. The 1-sigma uncertainty of the derived effective doses for the erythema and the vitamin D is estimated to be 5% since the contribution of photons with wavelengths shorter than 305 nm (where the signal may be very low) is small. However, the uncertainty in the calculated effective dose for the DNA-damage is larger at SZA greater than 60° because of the important contribution of shorter wavelengths (very low signal levels) and may reach 20% for SZAs near 80° in overcast conditions. The B086 provides measurements with a time frequency of 20 to 40 minutes, but atmospheric circumstances can change considerably within this period. It is therefore better to base the evaluation of the TEMIS UV dose rate (available at 10-minute intervals) on the NILU103 data, which have a better temporal resolution, thus they suffer much less from changes in atmospheric conditions (like clouds) during one measurement than the Brewer measurements.

3.2.2 Effective UV doses from NILU-UV irradiances using a neural network model

A feed-forward function-approximating NN model (Hornik et al., 1989) was coded using MATLAB's object-oriented scripting language in conjunction with its Neural Network Toolbox (Beale et al., 2012). As inputs, the NN has time series vectors of NILU103 irradiance measurements at 302, 312, 320, 340 and 380 nm together with temporal variables: the SZA, the day of the week (DOW), the day of the year (DOY) and its sinusoidal components $\sin(DOY \times 2\pi/T)$ and $\cos(DOY \times 2\pi/T)$ where T is the number of days in the year. As outputs, the NN calculates time series for the biological UV products resulting from B086 response weighted spectra: i.e. erythemal CIE, vitamin D and DNA-damage effective doses. The rationale behind including temporal variables in the inputs is that geophysical variables very often exhibit periodicity associated with an annual or diurnal cycle and are now commonly incorporated into atmospheric chemistry models (Kolehmainen et al., 2001). From the NILU103 data, a matrix of $n = 47{,}908$ co-located input-output vectors was extracted to train and validate the model. All output variables were found to correlate strongly and positively on all 5 of the irradiances ($0.922 \leq r \leq 0.995$),strongly anti-correlate with SZA ($-0.891 \leq r \leq -0.909$), and weakly anti-correlate with the temporal variables. Figure 2 shows the z-scores of the input variables and the erythemal UV dose (“CIE ”) together with the pairwise linear Pearson correlation coefficient.

The input and output vectors used in our study were connected via 2 network layers, the first containing hidden neurons with hyperbolic tangent ($tanh$) activation functions and the second containing linear activation functions. The mathematical details of this input-output structure is described in Appendix A. Key to the success of the modeling approach is signal to noise separation. The NN model is constructed using denoised time series of the NILU-UV irradiances and denoised time series of the photobiological products. Once constructed, the original (noisy) data is input to the model to calculate the photobiological outputs. In order to achieve this, we applied singular spectrum analysis to separate the signal (total trend plus periodicity) from the total noise component for each of the irradiance and photobiological product time series (see Ghil et al. (2002) for a review

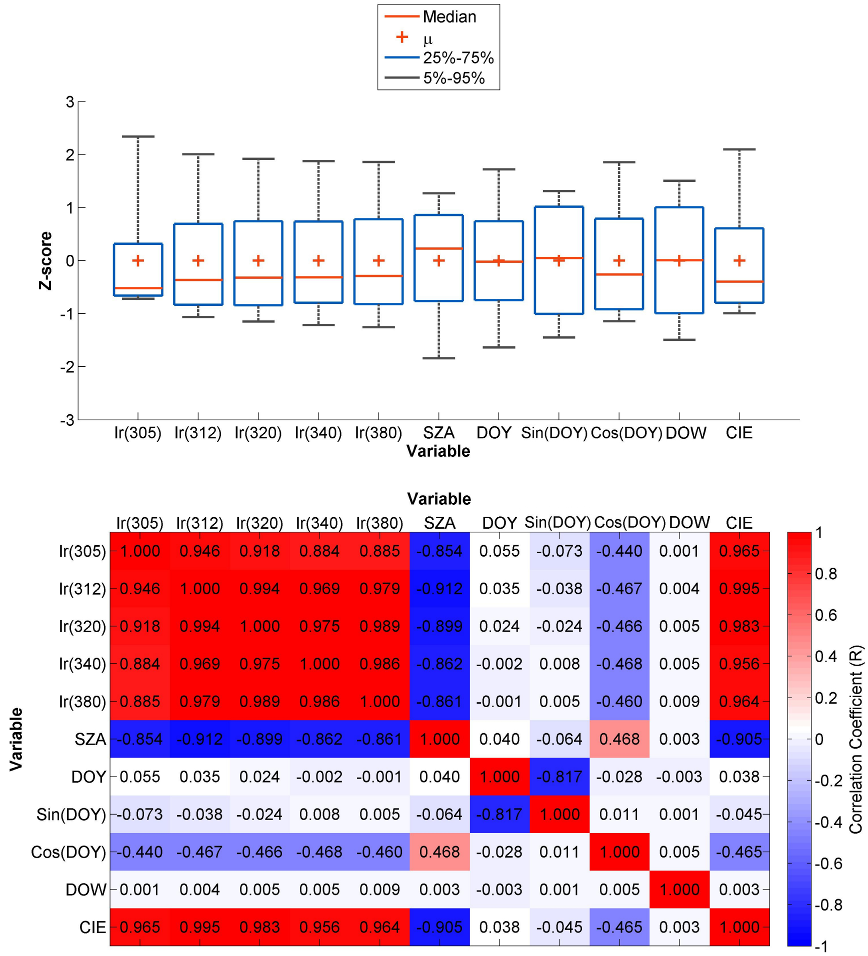

Figure 2. Model selection. (Top) ~~The~~ Boxplots of the z-scores of the input variables and the erythemal UV dose (CIE) with mean values denoted by μ. (Bottom) the pairwise linear Pearson correlation coefficient for each combination of the input variables and/or the output variable. The results are unnoticeably different in the case of Vitamin D and DNA damage doses. To save space, we have used abbreviated labeling of the sinusoidal terms so that $sin(DOY)$ refers explicitly to $sin(DOY \times 2\pi/T)$ etc.

of the singular spectrum analysis methodology). In this work we calculated the unbiased estimator for the lag-covariance matrix using the method of Vautard et al. (1992). The window length was rounded to ~~$log(n)^{1.5} = 36$~~ $[log(n)]^{1.5} = 36$ following the prescription of (Kahn and Poskitt, 2010) and the minimum distance length criterion they introduce was applied. This was found to give a consistent separation of the signal from noise for the NILU103 irradiance measurements at 302, 312, 320, 340 and 380 nm at eigenvalue ranks 9,7,7,5,5 respectively and in the case of the photobiological products, at eigenvalue ranks 7,8 and 8 respectively for CIE, vitamin D, DNA. This denoised data structure enables the NN model to determine the underlying

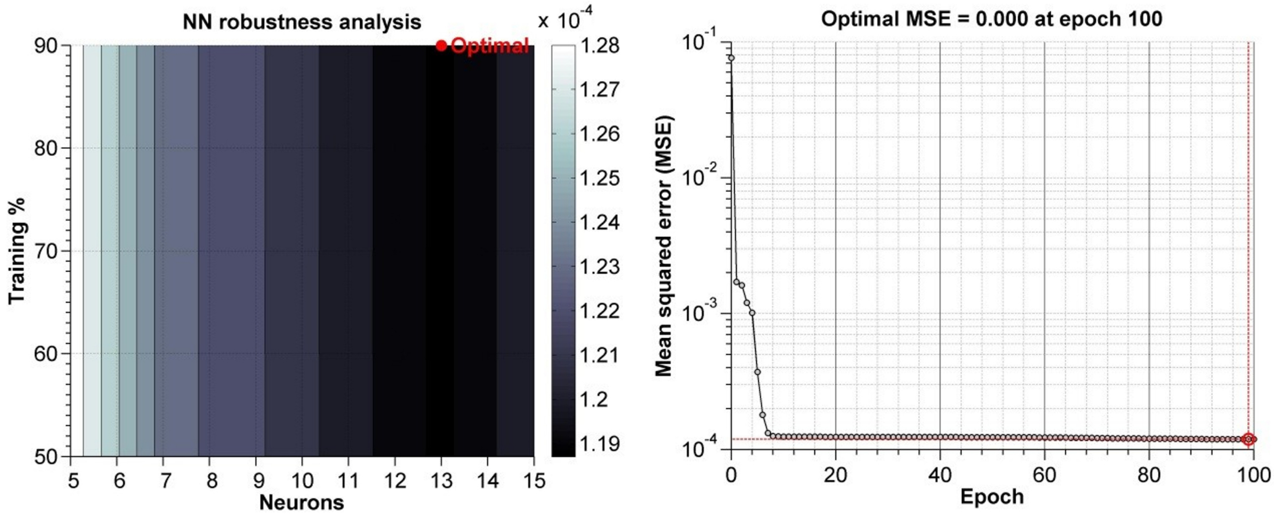

Figure 3. (Left) The robustness analysis on the grid of 100 NN models using the minimum validation MSE as the criterion for selection of the optimal NN architecture (which was found to have 13 hidden neurons and a training:validation data split of 90%:10%). (Right) The progress of the NN training of the optimal architecture with backpropagation iteration out to 100 iterations ("epochs") where $MSE < 1.0e^{-4}$.

relation between the input and output parameters most efficiently.

The optimal NN architecture was then found by minimizing the mean squared error (MSE) between the NN estimates and Brewer reference output data for each NN in a grid of 100 NN architectures where the number of hidden neurons was varied from 5 to 15 and the proportion of training data (t/n) was varied from 50% to 95% in steps of 5%. The subset of t-vectors was chosen randomly with a random number generator applied to the vector of indices $[1:n]$ and the remainder being used as a validation set that contained $(n-t)$ vectors. During each of 100 iterations of the learning process, the weights and biases of each NN are tuned with the back-propagation optimization algorithm (Rumelhart et al., 1986) to minimize the MSE cost function over the set of input-output vectors. We have used the Bayesian regularization scheme based on a Laplace prior (Foxall et al., 2002). As a result of this initial robustness analysis, the optimal NN was found to require 13 hidden neurons and a training to validation ratio of $90\% : 10\%$ as seen in Figure 3 which also shows the result of applying the model selection procedure as well as the progression of training of the optimal NN architecture towards convergence at the horizontal asymptote for the "best"validation MSE after 100 epochs of back-propagation learning using Bayesian regularization. Note that for the rather long time series used here, there is almost no visual dependence on the training fraction above 50% with a gradient in the optimization surface only being apparent in the direction of increasing number of neurons.

It is important to note that the optimal NN is valid for the range of parameters determined by the training data shown in Table~~1.~~ 1 . Temporal variables other than SZA are not listed and have the following expected ranges: DOY=[0,366], $\sin(DOY \times 2\pi/T) = [-1,1]$, $\cos(DOY \times 2\pi/T) = [-1,1]$ and DOW=[1,7].

Table 1. Range of validity of the trained optimal NN as determined by its input parameters (upper list) and output parameters (lower list).

Parameter	Min	Max	Mean	St. Dev.
Ir(302)	0	0.017	0.003	0.004
Ir(312)	0	0.229	0.064	0.055
Ir(320)	0	0.333	0.108	0.079
Ir(340)	0	0.678	0.252	0.159
Ir(380)	0	0.871	0.327	0.208
SZA	15.63	81.162	54.373	16.120
CIE	0	0.234	0.056	0.054
vitamin D	0	0.460	0.103	0.107
DNA	0	0.011	0.002	0.002

For validation, this optimally-trained NN was then fed with the remaining ("unseen") input vectors from the 10% of the training data and its estimates are compared against the target measurements of the output vector to evaluate the network performance. The correlation of NILU103 NN estimates with target outputs was high (r =0.988 to 0.990) and found to have a very low bias (0.000 to 0.011 absolute units) as shown in Figure 4. Neural-network-based estimates of retrieval uncertainty is still embryonic (see for example Ristovski et al. (2012)) due to the difficulty associated with propagating errors through a nonlinear function. In order to provide a ~~ballpark~~ rough estimate, we calculated the median absolute percentage error (MAPE) for the difference between the target values and the NN outputs and obtained the following estimates of the NN uncertainty: $\Delta(CIE) = 3.6\%$, $\Delta(VitaminD) = 4.5\%$ and $\Delta(DNA) = 5.1\%$. The uncertainties seen in the NILU NN products are well aligned with the uncertainties introduced by the NILU and B086 irradiances, 5.6% and 5% respectively. An estimation of the uncertainty lying into the ~~NILY~~ NILU NN products based on error propagation, results to absolute errors less than 7.5% for all three products.

3.2.3 Effective UV doses from the UVB-1 radiometer

~~The Yankee~~ As described in Sect 3.1, the measured doses by the YES UVB-1 radiometer ~~provides measurements of the erythemal dose rates whereas the dataset's validity is monitored by coincident measurements from the double monochromator B086. Using the effective doses derived from the~~ are converted to erythemal doses by applying proper correction factors which depend on the values of SZA and TOC for each measurement. The parametrization suggested by Fioletov et al. (2009) is then applied to convert the erythemal dose to vitamin D effective dose. Based on the measurements of B086 ~~, we adopted the empirical relationship suggested by Fioletov et al. (2009) to convert erythemal irradiance to effective dose for the formation~~

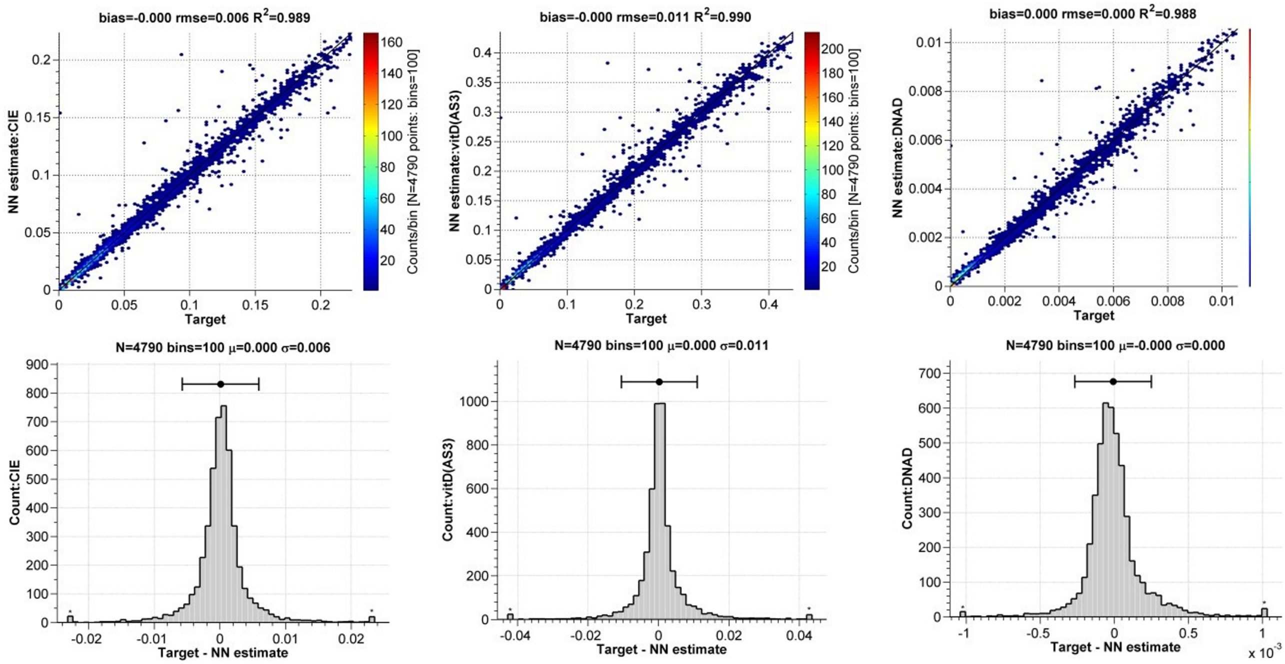

Figure 4. NN validation. (Upper Panels) Regression of the NILU103 NN estimates on the coincident Brewer-derived erythemal UV dose (CIE) (left), vitamin D (centre) and DNA-damage dose (right). (Lower Panels) Histograms of the difference between NN estimates and the Brewer-derived quantities. The mean (μ) and standard deviation (σ) are indicated.

~~of vitamin D , based on measurements of the total ozone column (TOC), and the cosine of the SZA. It was found that for UV index (UVI) values below~~ we found that when UV index is lower than 2, the vitamin D is overestimated significantly and should be divided by the following correction factor (cf) obtained empirically by a least squares fit to the data:

$$cf = -0.086 \cdot \mathrm{UVI}^{\,3} + 0.379 \cdot \mathrm{UVI}^2 - 0.575 \cdot \mathrm{UVI} + 1.317 \tag{5}$$

In a similar way, the DNA-damage effective doses were estimated from a more complex empirical relationship that was developed using data from B086 for the period $1993-2010$ and evaluated using data for the period $2011-2014$. The relationship for the DNA-damage effective doses consists of TOC, CIE, the cosine of the SZA ($cos\theta$) and the ratio between the CIE and the climatological value of CIE on each day and SZA (CIE_{clim}) :

$$DNA = g(TOC, \cancel{UVI}CIE, \cos\theta, \cancel{UVI}CIE_{clim}) = f(CIE, TOC)/(cf1(\cos\theta) \cdot cf2(r)) \tag{6}$$

Where:

$$r = CIE/CIE_{clim} \tag{7}$$

$$f(CIE,TOC) = \frac{a_1+s_2\cdot CIE+a_3\cdot CIE^2+a_4\cdot CIE^3+a_5\cdot CIE\cdot TOC+a_6\cdot CIE^3+a_7\cdot TOC\cdot CIE^2}{a_8\cdot CIE^2+a_9\cdot CIE+a_{10}} \frac{a_1+a_2\cdot CIE+a_3\cdot TOC+a_4\cdot CIE^2+}{a_8\cdot CIE} \tag{8}$$

$$cf1(cos\theta) = b_1 \cdot e^{b_2\cdot cos\theta} + b_3 \cdot e^{b_4\cdot cos\theta} \tag{9}$$

$$cf2(r) = \begin{cases} 1 & , \quad r > 2 \\ c_1 \cdot r^2 + c_2 \cdot r + c_3 & , \quad r \leq 2 \end{cases} \tag{10}$$

The values of the constant terms in Eqs 8 - 10 are: $a_1 = -2.703 \times 10^{-5}$, $a_2 = 0.01245$, $a_3 = 1.428 \times 10^{-8}$, $a_4 = 0.1151$, $a_5 = -1.736\times10^{-5}$, $a_6 = -0.1505$, $a_7 = -9.527\times10^{-5}$, $a_8 = -3.523$, $a_9 = 0.9388$, $a_{10} = 0.9611$, $b_1 = 1.022$, $b_2 = -3.994$, $b_3 = 0.7306$, $b_4 = 0.2755$, $c_1 = -0.3026$, $c_2 = 0.8971$, $c_3 = 0.401$. The empirical rule given by Eq. 6 was found to be valid for UVIs greater than 0.5. The daily mean TOC from the single monochromator B005 was used in the empirical equations and in cases of missing data, daily climatological means derived from the 30-year record of B005 were used. Using the effective doses from the double monochromator B086, we estimated that the 1-sigma uncertainty in the determination of vitamin D is smaller than 3% for UVI values greater than 2 and exceeds 10% for UVIs lower than 1. The 1-sigma uncertainty in the calculation of the effective dose for the DNA-damage is smaller than 7% for the range of used UVIs (i.e. greater than 0.5). The mean ratio between semi-simultaneous measurements of the clear sky erythemal irradiance from the B086 and the pyranometer ($\pm$ 1 minute differences between the mean time of the spectral scan and the UVB-1 measurements) for SZAs below 80°for the period $2004-2014$ is 1.00 ± 0.04, indicating that the uncertainty in the erythemal irradiance from the pyranometer is similar to that of the Brewer B086.

3.3 Comparison of the NILU-UV and UVB-1 data products

Following the appropriate methodologies already discussed in Sections 3.1 and 3.2, erythemal, vitamin D and DNA-damage daily doses can be obtained from the NILU103 and an erythemal-like measuring instrument, in this case a UVB-1 radiometer. Even though the UVB-1 data were corrected for the degradation of its absolute response with B086 data, the validity of its measurements as absolute values can be used to evaluate the performance of the NN used to derive all of the biological dose products based on NILU-UV measurements.

In order to have comparative results for the satellite data evaluations, daily doses of all three quantities under investigation were calculated and their agreement was evaluated. For these evaluations both the UVB-1 and the NILU103 one minute data were matched in order to avoid discrepancies due to random time gaps in the original time series. Then, the daily integrals were calculated for both NILU103 and UVB-1 datasets, without any other constrains on the data. The UVB-1 erythemal daily doses are underestimated on average by $\sim 2\%$ when compared to NILU103 retrievals, with a standard deviation of ~~5.39~~5.4%. When limiting the data to those during which more than 70~~%~~ % of the original measurements were classified as cloud free, the average agreement is close to perfect (average difference of ~~0.48~~0.5%) with a corresponding standard deviation of ~~4.21~~4.2%. This cloud classification criterion according to which days with more than 70% abundance of cloud free measurements are characterized as cloud free, is used throughout the study, unless stated otherwise. As seen in the lower panel of Figure 5(a), during the winter months UVB-1 tends to underestimate the erythemal daily doses, while during the summer months the ~~exact~~ opposite behaviour is observed.

The daily integrated data for vitamin D retrievals show that there is a good agreement between the UVB-1 and NILU103 sets. In both subsets, i.e. for all- and clear-skies, respectively, the standard deviations of the differences between the two datasets ~~are 7.43~~is 7.4% and 5%, respectively, while the differences between the datasets ~~are~~ is of the order of 4% for all skies and approaching zero (0.2%) for the cloud free days only. But, as observed in Figure 5(b), the number of cloud-free days is limited to only 25% of the originally available amount of days. Again, there is a seasonal pattern for Vitamin D which is similar to the seasonal pattern observed for the daily erythemal doses.

Concerning the DNA-damage daily doses (Figure 5(c)), the comparisons show that in general UVB-1 underestimates the daily dose on average by $\sim$5%, with a standard deviation of about 18%. For the cloud-free days, UVB-1 show an underestimation of $\sim$2% with a standard deviation of about $\sim$16%. The seasonal pattern observed at the lower level of Figure 5(c) is similar to the one depicted for the aforementioned daily doses but enhanced to $\pm$20%, especially for the winter months where the UVB-1 significantly underestimates the doses derived from NILU103.

In Table 2 an analytical overview of the NILU103 and UVB-1 comparison statistics is presented. All three quantities present high R^2 values (0.99 to 1.00), while the Pearson coefficients (R) reveal a strong linear correlation between the two ground-based datasets with values equal to almost unity. The DNA data are subjected to higher sensitivity in lower wavelengths and exhibit the largest differences between NILU103 and UVB-1.

Generally, the agreement between the two instruments is quite remarkable given the different nature of the original mea-

Table 2. Statistical analysis of the daily integral comparisons between NILU103 and UVB-1 retrievals.

Daily Integrals	Erythemal (%)		Vitamin D (%)		DNA-Damage (%)	
	All Skies	NILU clear	All Skies	NILU clear	All Skies	NILU clear
Ncounts	3013	731	3013	731	3013	731
R	0.998	0.996	0.998	0.996	0.997	0.997
R^2	1.00	0.99	1.00	0.99	0.99	0.99
Mean (%)	~~-1.85~~ -1.9	~~0.85~~ 0.9	~~-3.59~~ -3.6	~~0.20~~ 0.2	~~-4.82~~ -4.8	~~-2.26~~ -2.3
STD (%)	~~5.39~~ 5.4	~~4.21~~ 4.2	~~7.43~~ 7.4	~~5.00~~ 5.0	~~18.28~~ 18.3	~~16.39~~ 16.4

surements using different spectral resolution and different angular responses, which could be major parameters affecting the

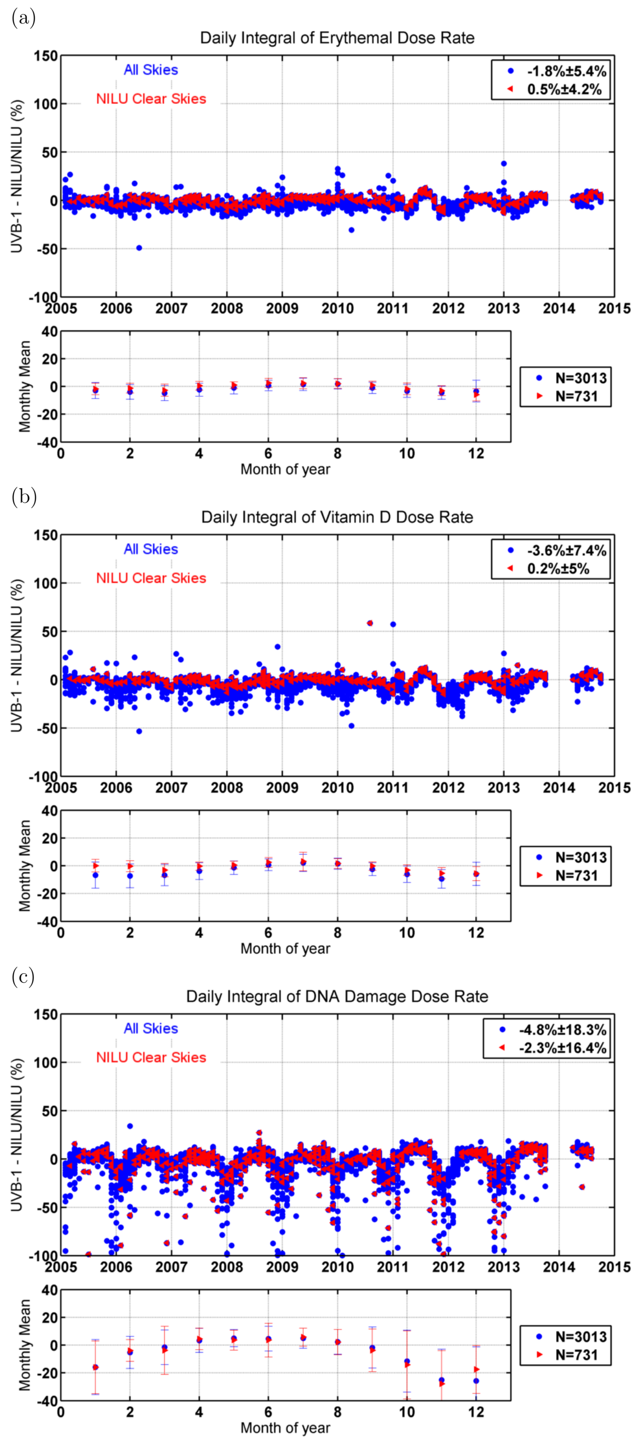

Figure 5. Daily integrals relative percentage differences of erythemal (a), vitamin D (b), and DNA-damage (c) doses estimates from the UVB-1 and NILU103 radiometers (upper panel) and the same datasets averaged on a monthly basis along with the 1-sigma error bars (lower panel).

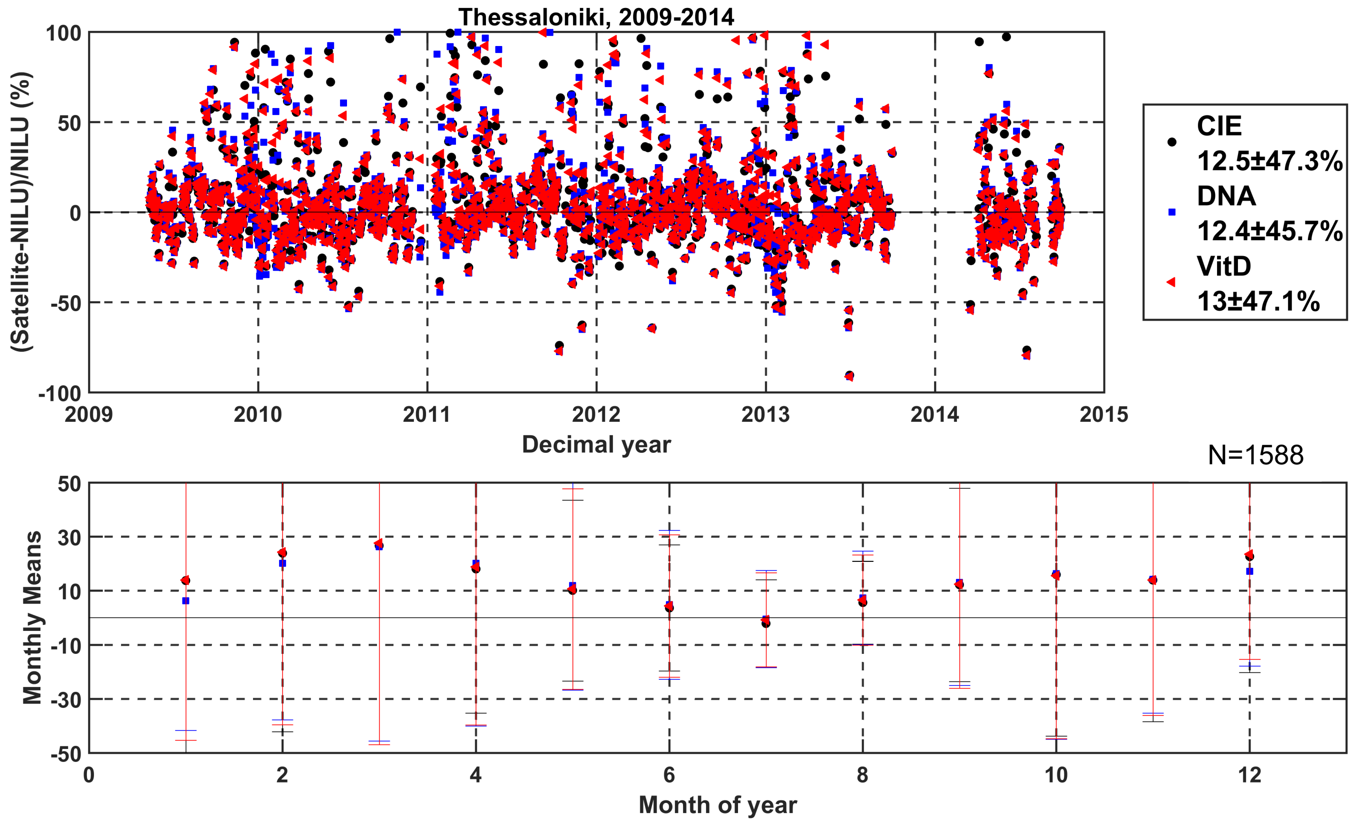

Figure 6. Time series of the relative percentage differences between the SCIAMACHY/GOME2A and NILU-UV effective daily doses under all skies (upper level) and the seasonality of the differences based on the average month along with the 1-sigma error bars (lower level).

comparisons, especially for the seasonal and SZA dependence, while the different retrieval methodologies could lead to further discrepancies.

4 Evaluation of TEMIS satellite-based UV products with NILU-UV data products

The satellite-based TEMIS UV products are evaluated for the grid cell containing Thessaloniki (grid cell centre: longitude = 22.75°, latitude = 40.75°). This evaluation uses a specifically reprocessed data set (version 1.4) to provide TEMIS UV dose rate values, calculated at the 10-min steps of the time integration of the daily dose UV products which are standard provided to the TEMIS data users. Time series analysis and correlation statistics are performed on the daily UV dose for erythema, vitamin D and DNA damage over a 6 year period (2009-2014). As seen in Figure 6 for all skies the TEMIS UV doses agree within 13% on average and achieve rather high correlations of 0.92, 0.93 and 0.93 for erythema, vitamin D and DNA-damage, respectively (Figure 7). The standard deviation of the differences for the three datasets ~~are 47.28%, 45.65~~under all skies is 47.3%, 45.7% and 47.1% for erythema, vitamin D and DNA-damage, respectively. The large variations between the satellite-based and ground-based UV daily dose data records can be attributed to different factors. For the full uncertainty budget contributions relate e.g. to the uncertainty in the B086 originally used spectra, the uncertainty caused by the application of the NILU-UV NN retrieval algorithm, the aerosol climatology assumed in the satellite-based algorithm and total ozone column retrieval errors. However, as will be demonstrated below, the greatest part of the observed spread in the ground-based and satellite-based differences in UV dose is related to the representation of clouds in the satellite algorithm and selection of cloud-free days for the ground-based data sets.

The NILU103 and TEMIS datasets have high coefficients of determination and low biases (small y-intercepts) as seen in Figure 7, while the slopes are close to unity. Although most points seem to cluster evenly around the $y = x$ line especially for the higher values, some overestimation of the satellite products at the lower values result in slopes that are slightly less than unity.

One important aspect for the evaluation is the determination of cloud-free days. The optical geometry of the two monitoring systems is different and the point measurements of the NILU at Thessaloniki compared to the $0.5° \times 0.5°$ spatial analysis of the satellite-based product may be an important source of discrepancies. Since the satellite-based estimates are based on only one total ozone column value throughout the day, we expect that this could further increase the uncertainty in the satellite-derived daily doses estimates.

Obviously, rapidly changing cloudiness conditions can also lead to large discrepancies between the ground and satellite retrievals. Currently the TEMIS satellite doses over Europe are obtained using the cloud cover fraction per $0.5° \times 0.5°$ grid cell as derived from SEVIRI/Meteosat cloud information. This information is incorporated in the TEMIS retrieval algorithm on a half-hourly basis, but the frequency of this information might need to be even higher when dealing with high frequency changing cloudiness conditions as shown in Figure 8 for two specific cloudy days at Thessaloniki. The time evolution illustrated for the two days in Figure 8 show that satellite cloud information cannot capture the rapid changes of cloudiness on these days: the satellite retrievals may either overestimate or underestimate the impact of clouds. Therefore, in order to evaluate the performance of the satellite-based products, the cloudiness effects should be further analyzed. Hereto, four different cases are examined in more detail: all skies cases (whose statistical analysis is given in Figure 6); days with more than 10% of the measurements characterized as cloud free (excluding overcast days); days with more than 70% of the measurements characterized as cloud free (relatively cloudless days); and days with more than 90% of the measurements characterized as cloud free (cloudless days). At this point it should be mentioned that for the characterization of the cloud free one-minute data, the cloud screening detector proposed by Zempila et al. (2016a) was applied on the NILU103 PAR measurements.

An overview of the impact in limiting the percentage of cloud-free cases per day (Ncl) is provided in Figure 9 for the erythemal UV doses. The relative percentage differences clearly improve considerably when excluding the overcast days (Ncl>10%). The original ~~12.46~~12.5% average overestimation of the satellite erythemal daily doses is reversed to ~~1.75~~1.8% underestimation, while the standard deviation is less than 15%. When posing the 70% limitation, as applied on the (UVB-1)-NILU comparisons in Section 3.3, the underestimation of the satellite erythemal doses seems to be even less while the standard deviation is similar. However, this limitation is affecting significantly the available number of days fulfilling this restriction through a reduction of

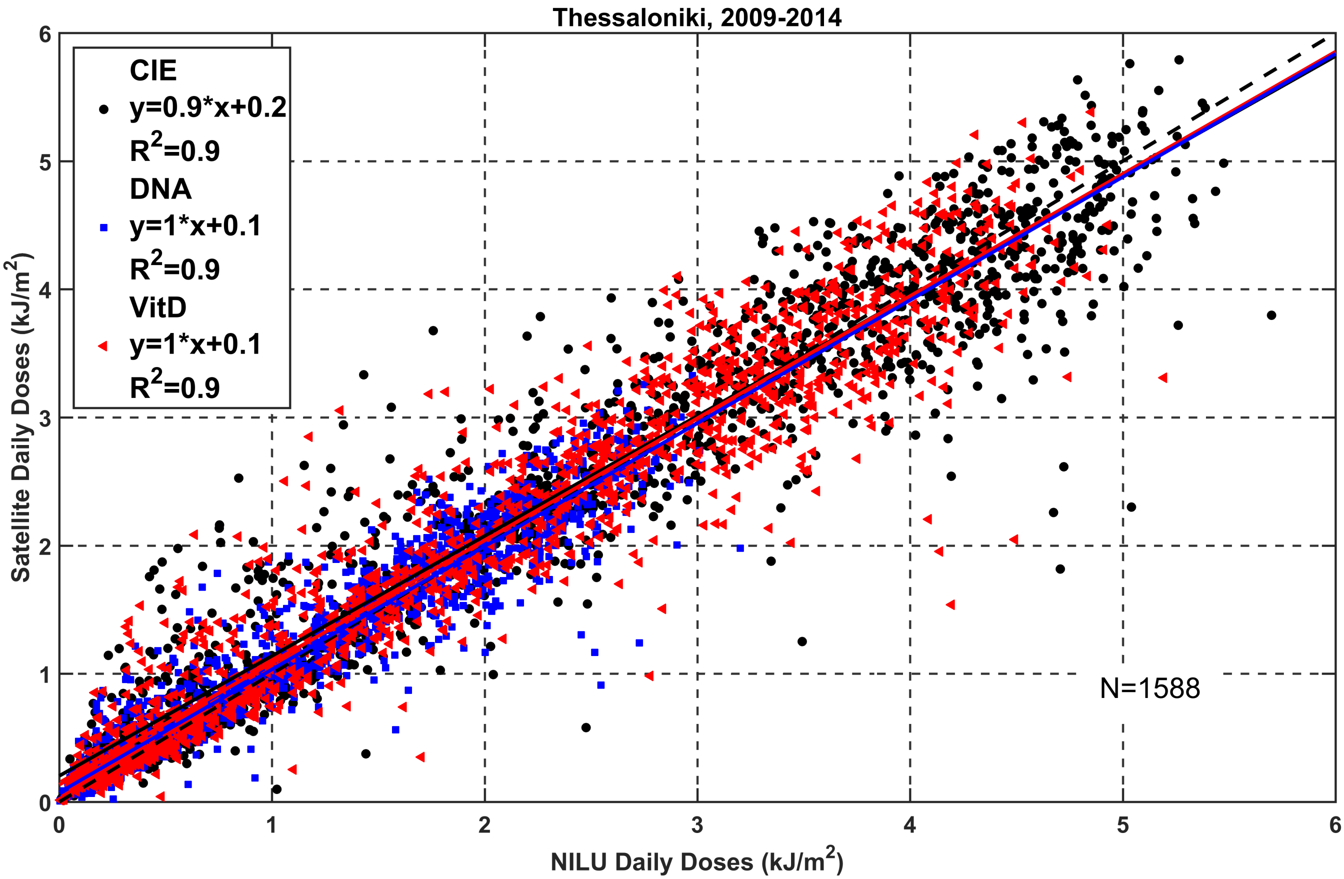

Figure 7. Scatter plot of daily UV dose values provided by the joint SCIA/GOME2A UV products (y-axis) and NILU103 (x-axis) in $\mathrm{kJ/m^2}$ under all skies conditions.

number of days by 75%. On the contrary, when studying the cloudless days (Ncl>90%), the satellite product is overestimated on average by only $\sim 0.6\%$ with a corresponding standard deviation of 11.5%. For these cloud free cases, the interpretation of aerosol effects into the satellite algorithm could be an additional parameter affecting these comparisons (see ~~bellow~~below).

A comprehensive statistical analysis of all three UV daily doses under investigation for all cloudiness conditions is provided in Table 3. All UV doses, erythemal, vitamin D and DNA-damage, respectively, present high R^2 values (≥ 0.9) for ~~either of~~ all the cloudiness restrictions, revealing a ~~highly linear relationship~~ high interconnection between the two datasets, while the correlation coefficients denote that under all circumstances, the UV effective doses present a high linear relationship . Although the satellite-based retrievals overestimate for all skies cases on average by ~~12.46~~12.5%, ~~13.04~~13.0% and ~~12.42~~12.4% for erythemal, vitamin D and DNA-damage respectively (Figure 6), the percentages are much smaller when considering only cloud-free days (in general less than 1.2%). Under mixed cloudiness conditions (Ncl>70% and >10%) satellite-based retrievals ~~on average~~ tend to underestimate the daily doses on average. As seen in table 3, the imposed cloudiness limitations do not alter

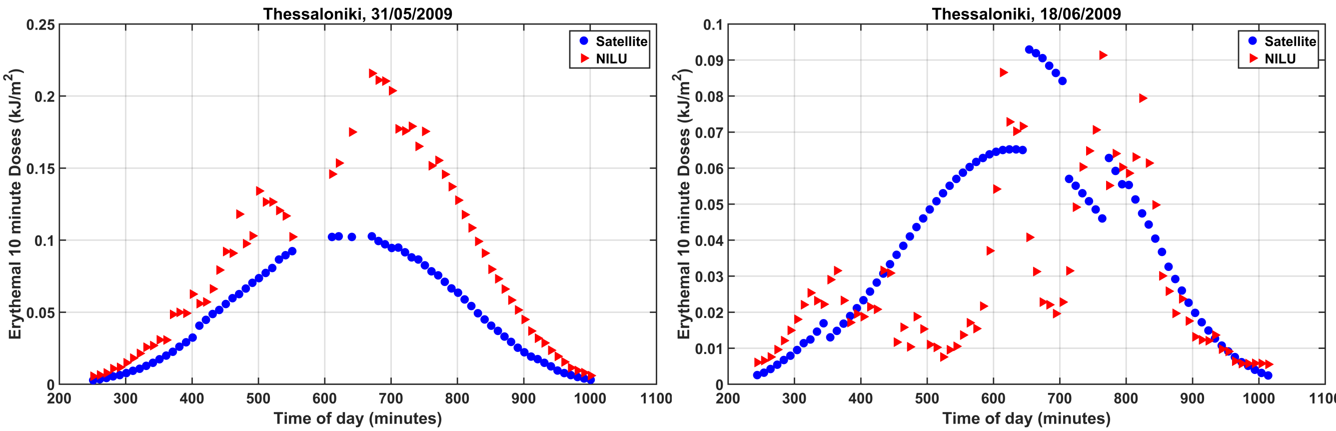

Figure 8. The evolution of the 10 minute erythemal dose over the day as provided by the satellite (blue circles) and at the ground (red triangles) for two days in 2009 showing a large temporal variability in cloudiness. The satellite-derived UV daily dose is lower than the NILU103-derived UV dose by 23% for the case on May, 30 2009 (left panel) while they are larger by 120% for the case on June, 18 2009 (right panel).

much the standard deviations.

Table 3 shows that even under cloud-free days there is a scatter of almost $\pm 13\%$ between the two datasets for all three UV

Table 3. Statistical analysis of the relative percentage differences [$(Satellite - Ground)/Ground\%$] between the satellite and ground estimates based on the cloudless instances within a day; The all skies values are given in Figures 6 and 7.

	Erythemal Doses			Vitamin D Doses			DNA-Damage Dos	
Cloudless instances per day (%)	>90%	>70%	>10%	>90%	>70%	>10%	>90%	>70%
Ncounts	203	390	991	203	390	991	203	390
R	0.96	0.95	0.95	0.96	0.95	0.95	0.96	0.95
R^2	0.92	0.9	0.9	0.92	0.91	0.91	0.92	0.91
Mean (%)	~~0.57~~ 0.6	~~-1~~ -1.0	~~-1.75~~ -1.7	~~1.22~~ 1.2	~~-0.36~~ -0.4	~~-1.40~~ -1.4	~~1.18~~ 1.2	~~-0.34~~ -0.3
STD (%)	~~11.47~~ 11.5	~~13.17~~ 13.2	~~14.18~~ 14.2	~~12.88~~ 12.9	~~14.48~~ 14.5	~~15.21~~ 15.2	~~12.18~~ 12.2	13.9

doses. The seasonality seen in Figure 6 is also present when limiting the datasets to cloud-free days, as seen in the lower panel of Figure 10, implying that apart from the cloud effects, there are other factors affecting the agreement between the ground- and satellite-based UV data products. One of the causes could be variability ~~in the~~ of aerosol load over Thessaloniki which is neglected in the satellite-based retrievals.

At Thessaloniki, AOD values at 340 nm are provided by a CIMEL sun photometer for the period 2011-2014.

In order to investigate the influence of aerosols on the satellite retrievals, estimations of all three UV effective doses every 10 minutes were obtained both from the satellite and NILU103 retrieval algorithms. These datasets were limited to periods

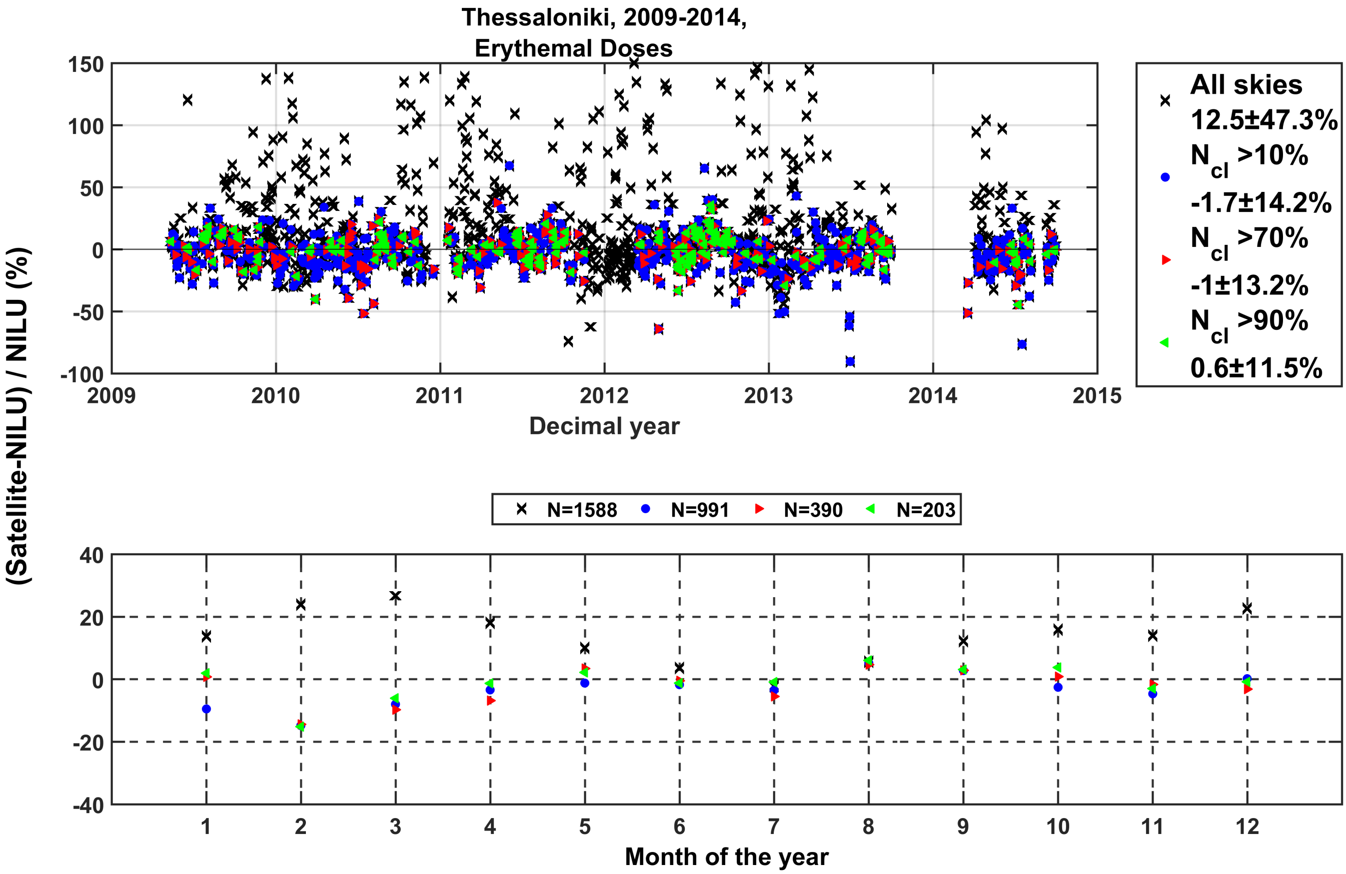

Figure 9. Time series of the relative differences between the satellite-based and ground-based retrieval of the UV erythemal doses; also a classification of the cloudless measurements per day is shown along with the corresponding statistics (upper panel). The seasonality of the data is presented also as monthly mean values (lower panel).

where the ground-based cloud screening algorithm resulted in cloud-free cases. As seen in the upper level of Figure 10 there is a strong dependence between the 10 minute doses for aerosol optical depth up to 0.4, while the differences show a slow ascending slope for aerosol loads of more than 0.4. To further testify on this aspect, linear fits were conducted for two datasets, one that comprised data with AOD≤0.4 and the second with data with corresponding AOD>0.4. It was found that for all three UV effective doses, the slopes for the first imposed limitation on AOD were higher than those calculated for the second dataset. Specifically, the slopes for the two AOD limitations were found to be 44.5% and 11.7% for the CIE, 50.6% and 8.5% for the DNA damage, 46.1% and 8.3% for the vitamin D doses respectively. This general pattern is in compliance with the implicit climatological AOD and SSA values applied in the satellite-based retrievals, where the AOD at 368 nm is assumed to be 0.3 and SSA is set to 0.9 (~~please see Section 2.2for further details)~~Section 2.2). To further investigate the AOD impact on the comparisons, the monthly means were calculated for both AOD and relative differences. The pattern seen in the monthly means of the AOD values is in general agreement with the seasonality seen in the average monthly values of the relative percentage

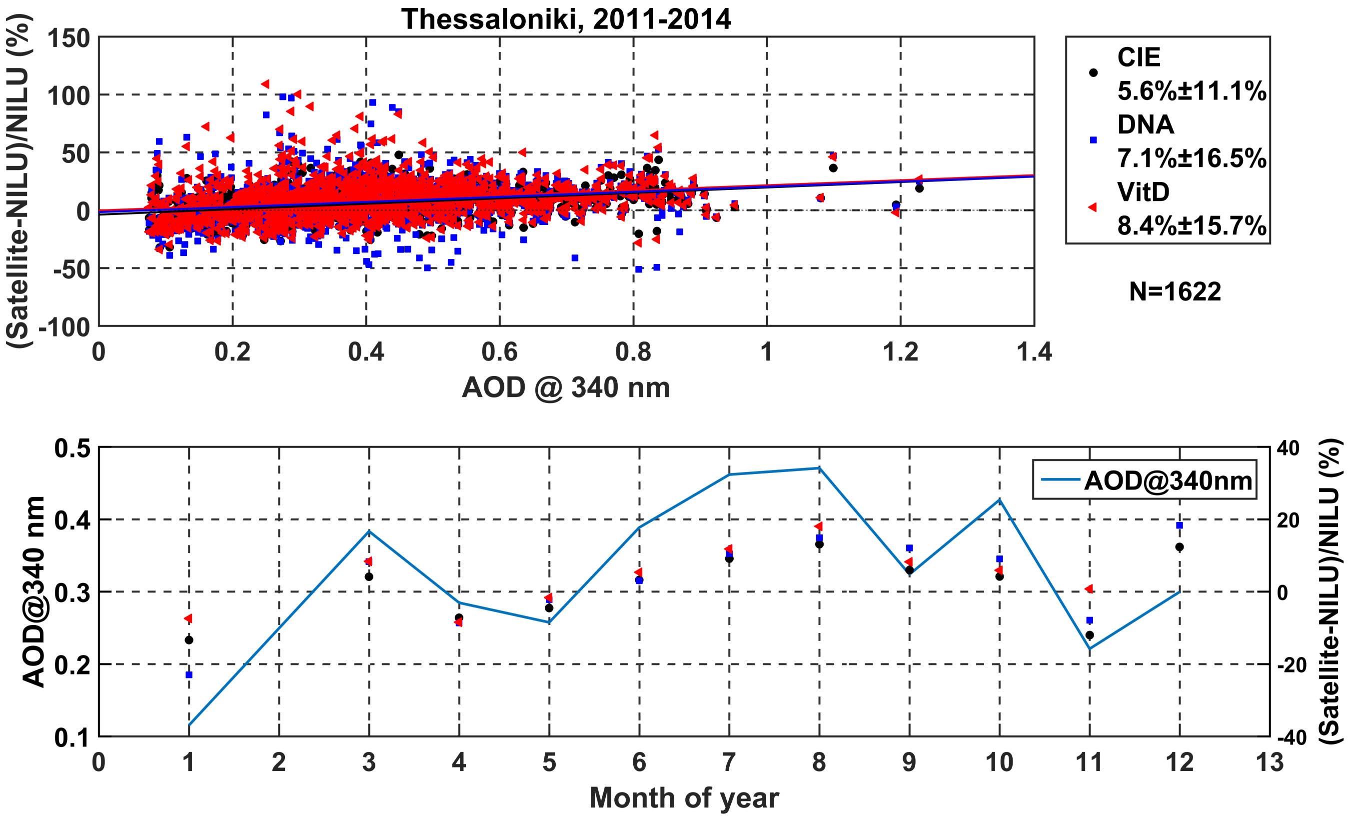

Figure 10. Relative differences of satellite-based and ground-based UV ~~daily~~ 10-minute doses as a function of AOD at 340 nm for cloudless ~~days~~ cases at Thessaloniki in the period 2011-2014. The statistics are provided in the form of mean and standard deviation of the differences (upper panel). Monthly mean values of AOD at 340 nm along with the mean monthly values of the relative differences presented in the upper panel under cloud free cases, are also provided (lower panel).

differences between the satellite- and ground-based 10-minute cloudless doses (Figure 10, lower panel), implying that there is a link between the two observed seasonalities.

Model estimations performed with the model uvspec of the libRadtran library (v. 1.7) reveal that for typical aerosol optical properties for the site of Thessaloniki, differences of 0.2 between the AOD values used in the ground-based retrieval algorithm and the measured AOD, may be responsible for differences of the order of 10% between the measured and retrieved erythemal dose rates. Furthermore, other aerosol properties, like the single scattering albedo, may vary significantly over urban sites such as Thessaloniki (Bais et al., 2005) which can introduce extra uncertainties in the effect of aerosols on the estimated UV irradiances which are of the same order of magnitude as the uncertainty due to the variability in the AOD (e.g. Kazadzis et al., 2009; Fountoulakis et al., 2016a).

5 Discussion and Conclusions

In this work a cross-validation between ground-based measurements and evaluation of TEMIS satellite-based estimates has been performed for three important photobiological UV daily dose products: erythemal UV, vitamin D and DNA damage. The data sets to compare have been produced and compiled such to allow ~~thoroughly~~ a thorough discussion of their respective accuracies and limitations at the mid-latitude UV and ozone monitoring station in the Laboratory of Atmospheric Physics of the Aristotle University of Thessaloniki, Greece. A neural network (NN) algorithm has been trained on NILU-UV multi-filter radiometer irradiances at 5 different wavelengths together with weighted action-spectra from a Brewer MKIII spectrophotometer to produce 1-minute time series of erythemal UV, vitamin D and DNA-damage dose rates. Further, the NN estimated erythemal UV dose rates were compared with UVB-1 calibrated UV measurements and we show how appropriate methodologies can be applied to the original UVB-1 data set to also produce vitamin D and DNA-damage dose rates at the same temporal resolution as the NILU-UV instrument. In this way we could perform a ground-based verification and evaluation of the developed NN algorithm for the NILU103 measurements. The cross-validation between the NILU103 and the UVB-1 dataset revealed a very good agreement. In particular, it is found that:

- The temporally aligned NILU-UV NN and UVB-1 ground-based datasets (30,503 coincident ‘all skies’ dose rate data records) did not show differences of more than 2% in their daily integrals and these also had a moderately low standard deviation of ~~5.39~~5.4%.

- For vitamin D, the agreement was within 3.6% for all skies data with a standard deviation of about 7.4%, largely associated with a SZA dependence at large zenith angles. For cloud-free days this effect is reduced to about 5.0%.

- The DNA dose rates, the most demanding of the three doses discussed in this study because of their sensitivity to short wavelengths in the UV spectral region, agree to within about 5%, dropping to ~~2.26~~2.3% for the cloud free cases.

For the evaluation of the satellite-based TEMIS UV products with the NILU-UV derived ground-based products it is found in particular that:

- The TEMIS UV daily dose products are, on average, 12.5% higher than the NILU103 daily doses under all skies. Despite the presence of a visually apparent seasonal pattern, the correlation was found to be robustly high ($R^2 = 0.92$ and $R = 0.95$).

- For the vitamin D (DNA-damage) UV daily doses the differences under all skies cases between the satellite- and ground-based estimates are similar with differences of on average 13% (12.5%), again with the satellite overestimating the dose and again with very good correlation of $R^2 = 0.93$ and $R = 0.95$ ($R^2 = 0.93$ and $R = 0.95$).

It is well possible that the implicit aerosol climatology used in the satellite retrieval algorithm is at least partly contributing to higher UV doses at a moderately polluted site as Thessaloniki. Further, in the shorter wavelength part of the UV-B spectral region errors in measuring the total ozone column can have a relatively higher impact for an accurately retrieval of the DNA-damage UV dose and Vitamin D UV dose compared to the erythemal UV dose. However, the ratios and the standard deviations for the differences in the three UV doses are similar, suggesting that the contribution of errors related to the total ozone column retrieval may not be very important. Uncertainties in the B086 spectra and the methodologies used for the calculation of the Vitamin D and DNA-damage effective doses might also be partly responsible for the observed variability, but these factors only can explain a small fraction of the total variability in the differences (in general less than 7% for all skies conditions).

Through data selections for different cloud cover conditions it was shown that the greatest part of the variability is due to the differences between the cloud cover fraction assumed in the satellite algorithm and the definition of cloud-free cases in the ground-based retrievals because the different field of view between the ground- and satellite-based instruments might lead to discrepancies regarding the cloud influences on the UV daily doses. Three clusters of cloudiness types were investigated in order to evaluate the cloud contribution on the differences between the satellite- and ground-based UV daily doses. The introduced clusters were identified based on the percentage of cloud-free ~~moments~~ periods over a day: excluding overcast days (days with more than 10% cloudless measurements), moderate cloud-free days (days with more than 70% cloudless measurements), and cloud-free days (days more than 90% cloudless measurements).

- The number of cloud-free days limits the dataset ~~by almost 75% and the~~ to one fourth of the original, while the mean relative differences are reduced for all daily UV doses. Remaining discrepancies are on average less than 1.3% for the Vitamin D and DNA-damage doses, while the agreement for erythemal UV is on average even smaller (~~0.57~~0.6%), revealing the notable improvement of the comparisons when excluding the cloudiness effects.

- Differences of less than 2% with moderate standard deviations (∼15%) are found when excluding the overcast days, implying that the major source of the high differences observed under all skies cases can be attributed to the availability and treatment of the cloud information, e.g. the satellite algorithm cannot distinguish between thin and thick clouds under overcast conditions

Finally, the influence of aerosol variability was investigated using the UV doses from the cloud-free days only. Coincident AOD values at 340 nm from a collocated CIMEL sunphotometer were used in order to examine the dependence of the observed differences to the aerosol load at the urban site in Thessaloniki. The results showed that for AOD values up to 0.4 the contribution of aerosols to the differences in UV dose is quite significant while for even larger AOD this contribution results to slowly ascending slops. Furthermore, model estimations demonstrated that discrepancies between the measured and assumed SSA values can also lead to high differences on the retrieved irradiances which are equivalent to those attributed to the variability of AOD. Thus the discrepancies seen in the two datasets under cloud free conditions can be at least partly attributed to the implicit aerosol information used in the satellite retrievals at the site of Thessaloniki which experiences significant variations in aerosol properties.

In conclusion, this comprehensive study has revealed the merits, limitations and accuracy of both ground-based and satellite-based estimates of erythemal UV, vitamin D and DNA-damage daily doses and underlying dose rates. Although calibration procedures, a-priori information and constraints of the methods applied in the original datasets can still limit the accuracy of the calculated photobiological products, these types of data comparisons will remain highly important for the validation of satellite-derived UV doses and to further increase the awareness of the harmful effects of overexposure to UV radiation.

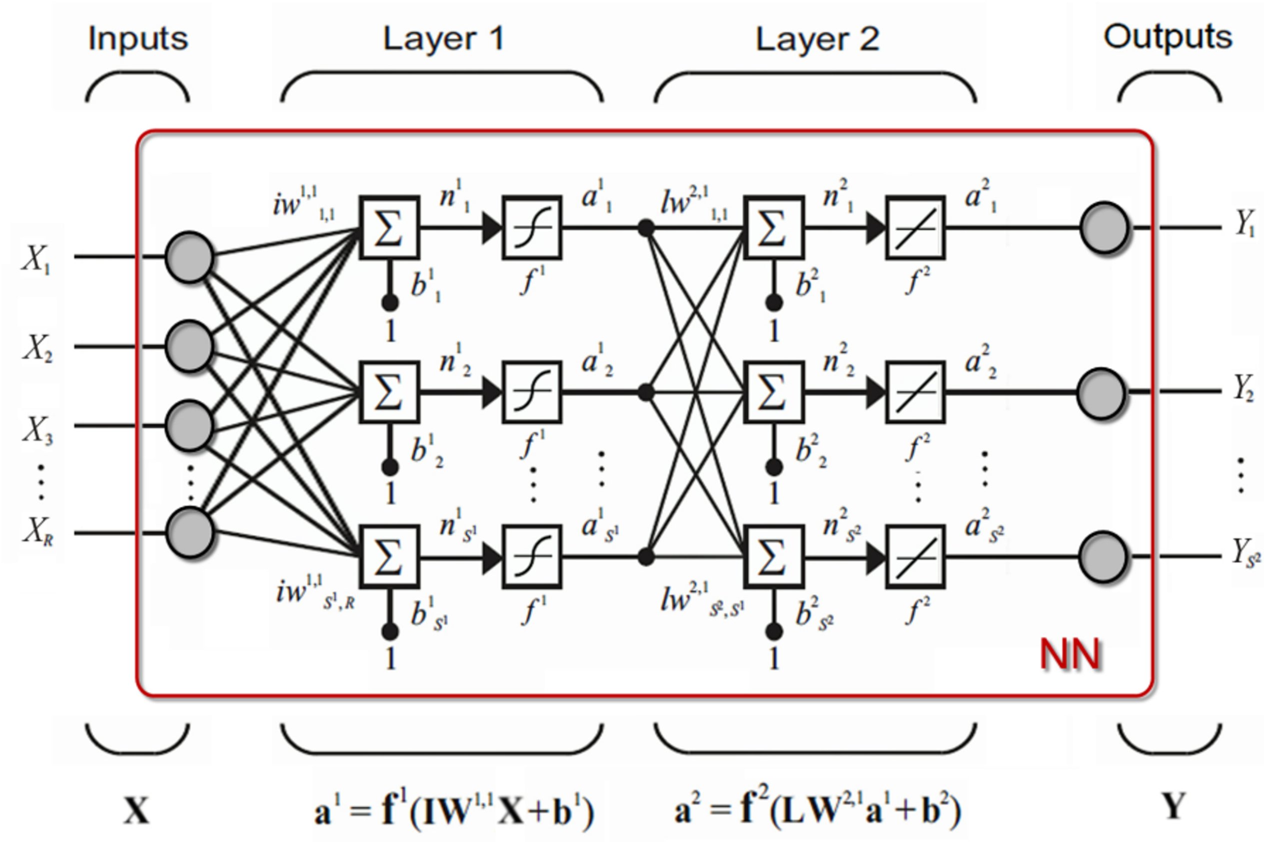

Figure 11. Schematic showing the neural connectivity between input and output parameters in the NILU-UV NN model.

Appendix A: Neural Network input-output theory

The mathematical structure of the neural network model used in this work is described here.

The NN connects a 10-parameter input vector $X = [Ir(302), Ir(312), Ir(320), Ir(340), Ir(380), SZA, DOY, \sin(DOY \times 2\pi/T), \cos(DOY \times 2\pi/T), DOW]^T$ through 2 layers of neurons to a 3-parameter output vector $Y = [CIE, vitaminD, DNA]^T$. Layer 1 (the ~~“hidden”~~ "hidden" layer) contains $\cancel{s^1}$ $s^1 = 13$ neurons each having a nonlinear activation function $f^1 = tanh$ and Layer 2 (the ~~“~~"output" layer) contains $\cancel{s^2}$ $s^2 = 3$ neurons each having a linear activation function f^2. Each neuron also has a single bias [0,1]. a^1 is the vector of outputs from Layer 1 and a^2 is the vector of outputs from Layer 2. The vector X is therefore connected to the hidden layer via a matrix of input weights $IW^{1,1}$ of size $[s^1 \times R]$ and the output of the hidden layer is connected to s^2 output neurons via a matrix of layer weights $LW^{2,1}$ of size $[s^2 \times s^1]$. The vector a^2 for the s^2-outputs in vector Y is the output of the NN model. The exact mathematical equation relating the outputs to the inputs is represented by the matrix equation (Taylor et al., 2014):

$$Y = f^2(LW^{2,1} f^1(IW^{1,1} X + b^1) + b^2). \quad \text{(A1)}$$

Note that the multiplication of the matrix $IW^{1,1}$ and the vector X is a dot product and is equivalent to the summation over all input connections to each neuron in the hidden layer.

Acknowledgements. The authors would like to acknowledge the National Network for the Measurement of Ultraviolet Solar Radiation, uvnet.gr. The authors would also like to express their gratitude to Marc Allaart of KNMI for his kind support to the TEMIS algorithm development.

References

Allaart, M., van Weele, M., Fortuin, P., and Kelder, H.: An empirical model to predict the UV-index based on solar zenith angles and total ozone, Meteorological Applications, 11, 59–65, 2004.

Badosa, J. and van Weele, M.: Effects of aerosols on UV index, Tech. Rep. WR-2002-07, KNMI, De Bilt, 2002.

Bais, A., Zerefos, C., Ziomas, I., Zoumakis, N., Mantis, H., Hofmann, D., and Fiocco, G.: Decreases in the Ozone and the S02 Columns Following the Appearence of the El Chichon Aerosol Cloud at Midlatitude, in: Atmospheric Ozone, pp. 353–356, Springer, 1985.

Balis, D., Giannakaki, E., Müller, D., Amiridis, V., Kelektsoglou, K., Rapsomanikis, S., and Bais, A.: Estimation of the microphysical aerosol properties over Thessaloniki, Greece, during the SCOUT-O3 campaign with the synergy of Raman lidar and Sun photometer data, Journal of Geophysical Research: Atmospheres, 115, n/a–n/a, doi:10.1029/2009JD013088, http://dx.doi.org/10.1029/2009JD013088, d08202, 2010.

Beale, M. H., Hagan, M. T., and Demuth, H. B.: Neural network toolbox user's guide, in: R2012a, The MathWorks, Inc., 3 Apple Hill Drive Natick, MA 01760-2098,, www. mathworks. com, Citeseer, 2012.

Bernhard, G. and Seckmeyer, G.: Measurements of spectral solar UV irradiance in tropical Australia, J. Geoph. Res., 102, 8719–8730, doi:10.1029/97JD00072, 1997.

Berwick, M., Armstrong, B. K., Ben-Porat, L., Fine, J., Kricker, A., Eberle, C., and Barnhill, R.: Sun exposure and mortality from melanoma, Journal of the National Cancer Institute, 97, 195–199, 2005.

Boersma, K. F., Eskes, H. J., and Brinksma, E. J.: Error analysis for tropospheric NO_2 retrieval from space, J. Geophys. Res., 109, 20 pp., doi:10.1029/2003JD003962, 2004.

Bouillon, R., Eisman, J., Garabedian, M., Holick, M., Kleinschmidt, J., Suda, T., Terenetskaya, I., and Webb, A.: Action spectrum for the production of previtamin D3 in human skin, UDC, 612, 481–506, 2006.

Bovensmann, H., Burrows, J. P., Buchwitz, M., Frerick, J., Noel, S., Rozanov, V. V., Chance, K. V., and Goede, A. P. H.: SCIAMACHY: Mission objectives and measurement modes, J. Atmos. Sci., 56, 127–150, doi:10.1175/1520-0469(1999)056<0127:SMOAMM>2.0.CO;2, 1999.

Derrien, M. and Le Gléau, H.: MSG/SEVIRI cloud mask and type from SAFNWC, Int. J. Remote Sensing, 26, 4707–4732, doi:10.1080/01431160500166128, 2005.

Emde, C., Buras-Schnell, R., Kylling, A., Mayer, B., Gasteiger, J., Hamann, U., Kylling, J., Richter, B., Pause, C., Dowling, T., et al.: The libRadtran software package for radiative transfer calculations (version 2.0. 1), Geoscientific Model Development, 9, 1647–1672, 2016.

Engelsen, O., Brustad, M., Aksnes, L., and Lund, E.: Daily duration of vitamin D synthesis in human skin with relation to latitude, total ozone, altitude, ground cover, aerosols and cloud thickness, Photochemistry and photobiology, 81, 1287–1290, 2005.

Eskes, H. J., van Velthoven, P. F. J., Valks, P. J. M., and Kelder, H. M.: Assimilation of GOME total ozone satellite observations in a three-dimensional tracer transport model, Q. J. R. Meteorol. Soc., 129, 1663–1681, doi:10.1256/qj.02.14, 2003.

Fioletov, VE and McArthur, LJB and Mathews, TW and Marrett, L.: On the relationship between erythemal and vitamin D action spectrum weighted ultraviolet radiation, Journal of Photochemistry and Photobiology B: Biology, 95, 1, 9–16, 2009.

Fountoulakis, I., Bais, A. F., Fragkos, K., Meleti, C., Tourpali, K., and Zempila, M. M.: Short-and long-term variability of spectral solar UV irradiance at Thessaloniki, Greece: effects of changes in aerosols, total ozone and clouds, Atmospheric Chemistry and Physics, 16, 2493–2505, 2016a.

Fountoulakis, I., Redondas, A., Bais, A. F., Rodriguez-Franco, J., Fragkos, K., and Cede, A.: Dead time effect on the Brewer measurements: correction and estimated uncertainties, Atmospheric Measurement Techniques, 9, 1799–1816, 2016b.

Foxall, R. J., Cawley, G. C., Dorling, S. R., and Mandic, D. P.: Error functions for prediction of episodes of poor air quality, in: International Conference on Artificial Neural Networks, pp. 1031–1036, Springer, 2002.

Garane, K., Bais, A., Kazadzis, S., Kazantzidis, A., and Meleti, C.: Monitoring of UV spectral irradiance at Thessaloniki (1990? 2005): data re-evaluation and quality control, in: Annales Geophysicae, vol. 24, pp. 3215–3228, 2006.

Ghil, M., Allen, M., Dettinger, M., Ide, K., Kondrashov, D., Mann, M., Robertson, A. W., Saunders, A., Tian, Y., Varadi, F., et al.: Advanced spectral methods for climatic time series, Reviews of geophysics, 40, 1–41, 2002.

Hassinen, S., Balis, D., Bauer, H., Begoin, M., Delcloo, A., Eleftheratos, K., Gimeno Garcia, S., Granville, J., Grossi, M., Hao, N., Hedelt, P., Hendrick, F., Hess, M., Heue, K.-P., Hovila, J., Jønch-Sørensen, H., Kalakoski, N., Kauppi, A., Kiemle, S., Kins, L., Koukouli, M. E., Kujanpää, J., Lambert, J.-C., Lang, R., Lerot, C., Loyola, D., Pedergnana, M., Pinardi, G., Romahn, F., van Roozendael, M., Lutz, R., De Smedt, I., Stammes, P., Steinbrecht, W., Tamminen, J., Theys, N., Tilstra, L. G., Tuinder, O. N. E., Valks, P., Zerefos, C., Zimmer, W., and Zyrichidou, I.: Overview of the O3M SAF GOME-2 operational atmospheric composition and UV radiation data products and data availability, Atmospheric Measurement Techniques, 9, 383–407, doi:10.5194/amt-9-383-2016, http://www.atmos-meas-tech.net/9/383/2016/, 2016.

Herman, J. R. and Celarier, E. A.: Earth surface reflectivity climatology at 340-380 nm from TOMS data, J. Geophys. Res., 102, 28 003–28 011, doi:10.1029/97JD02074, 1997.

Holick, M., Bouillon, R., Eisman, J., Garabedian, M., Kleinschmidt, J., Suda, T., Terenetskaya, I., and Webb, A.: Action spectrum for production of previtamin D3 in human skin, Tech. Rep. final draft report of September 2005, CIE Technical Committee 6-54, 2005.

Hornik, K., Stinchcombe, M., and White, H.: Multilayer feedforward networks are universal approximators, Neural networks, 2, 359–366, 1989.

Kahn, M. A. R. and Poskitt, D S..: A note on window length selection in singular spectrum analysis, Australian & New Zealand Journal of Statistics, 55, 2, 87–108, 2013.

Kazantzidis, A., Bais, A. F., Topaloglou, C., Garane, K., Zempila, M. M., Meleti, C., and Zerefos, C.: Quality assurance of the Greek UV Network: preliminary results from the pilot phase operation,Proc. SPIE 6362, Remote Sensing of Clouds and the Atmosphere XI, 636229, 2006.

Kazantzidis, A., Bais, A. F., Zempila, M. M., Kazadzis, S., Peter, N., Koskela, T., and Slaper, H.: Calculations of the human vitamin D exposure from UV spectral measurements at three European stations, Photochemical & Photobiological Sciences, 8, 45–51, 2009.

Koelemeijer, R. B. A., De Haan, J. F., and Stammes, P.: A database of spectral surface reflectivity in the range 335-772 nm derived from 5.5 years of GOME observations, J. Geophys. Res., 108, 4070–4082, doi:10.1029/2002JD002429, 2003.

Kolehmainen, M., Martikainen, H., and Ruuskanen, J.: Neural networks and periodic components used in air quality forecasting, Atmospheric Environment, 35, 815–825, 2001.

Lantz, K. O., Disterhoft, P., DeLuisi, J. J., Early, E., Thompson, A., Bigelow, D., and Slusser, J.: Methodology for deriving clear-sky erythemal calibration factors for UV broadband radiometers of the US Central UV Calibration Facility, Journal of Atmospheric and Oceanic Technology, 16, 1736–1752, 1999.

MacLaughlin, J. A., Anderson, R., and Holick, M. F.: Spectral character of sunlight modulates photosynthesis of previtamin D3 and its photoisomers in human skin, Science, 216, 1001–1003, 1982.

McKenzie, R. L., Liley, J. B., and Björn, L. O.: UV radiation: balancing risks and benefits, Photochemistry and Photobiology, 85, 88–98, 2009.

McKinlay, A. and Diffey, B.: A reference action spectrum for ultraviolet induced erythema in human skin, CIE j, 6, 17–22, 1987.

Meleti, C., Fragkos, K., Bais, A., Tourpali, K., Balis, D., and Zerefos, C.: Thirty years of total ozone measurements at Thessaloniki with a MKII Brewer spectrophotometer, in: Quadrennial Ozone Symposium, 2012.

Parkin, D., Mesher, D., and Sasieni, P.: Cancers attributable to solar (ultraviolet) radiation exposure in the UK in 2010, British journal of cancer, 105, S66–S69, 2011.

Pope, S. J., Holick, M. F., Mackin, S., and Godar, D. E.: Action Spectrum Conversion Factors that Change Erythemally Weighted to Previtamin D3-weighted UV Doses, Photochemistry and photobiology, 84, 1277–1283, 2008.

Ristovski, K., Vucetic, S., and Obradovic, Z.: Uncertainty analysis of neural-network-based aerosol retrieval, IEEE Transactions on Geoscience and Remote Sensing, 50,2,409–414,2012.

Rumelhart, D., Hinton, G., and Williams, R.: Learning representations by back-propagation errors, Nature, 323, 533–536, 1986.

Samanek, A. J., Croager, E. J., Gies, P., Milne, E., Prince, R., McMichael, A. J., Lucas, R. M., and Slevin, T.: Estimates of beneficial and harmful sun exposure times during the year for major Australian population centres, Medical journal of Australia, 184, 338, 2006.

Setlow, R. B.: The wavelengths in sunlight effective in producing skin cancer: a theoretical analysis, Proceedings of the National Academy of Sciences, 71, 3363–3366, 1974.

Slaper, H., Reinen, H., Blumthaler, M., Huber, M., and Kuik, F.: Comparing ground-level spectrally resolved solar UV measurements using various instruments: A technique resolving effects of wavelength shift and slit width, Geophysical Research Letters, 22, 2721–2724, 1995.

Taylor, M., Kazadzis, S., Tsekeri, A., Gkikas, A., and Amiridis, V.: Satellite retrieval of aerosol microphysical and optical parameters using neural networks: a new methodology applied to the Sahara desert dust peak, Atmospheric Measurement Techniques, 7, 3151–3175, 2014.

van der A, R. J., Allaart, M. A. F., and Eskes, H. J.: Extended and refined multi sensor reanalysis of total ozone for the period 1970-2012, Atmos. Meas. Tech., 8, 3021–3035, doi:10.5194/amt-8-3021-2015, 2015.

van Geffen, J., van der A, R., van Weele, M., Allaart, M., and Eskes, H.: Surface UV radiation monitoring based on GOME and SCIAMACHY, in: Proceedings of the ENVISAT & ERS Symposium, 6-10 September 2004, Salzburg, Austria, SP 572, p. 8 pp., ESA, Paris, 2004.

van Weele, M., van der A, R. J., van Geffen, J., and Roebeling, R.: Space-based surface UV monitoring for Europe using SCIAMACHY and MSG, in: Proceedings of the 12th SPIE International Symposium on Remote Sensing, 19-22 September 2005, Bruges, Belgium, p. 8 pp., SPIE, 2005.

Vautard, R., Yiou, P., and Ghil, M.: Singular-spectrum analysis: A toolkit for short, noisy chaotic signals, Physica D: Nonlinear Phenomena, 58, 95–126, 1992.

Webb, A. R. and Engelsen, O.: Calculated ultraviolet exposure levels for a healthy vitamin D status, Photochemistry and Photobiology, 82, 1697–1703, 2006.

Webb, A. R., Kline, L., and Holick, M. F.: Influence of Season and Latitude on the Cutaneous Synthesis of Vitamin D3: Exposure to Winter Sunlight in Boston and Edmonton Will Not Promote Vitamin D3 Synthesis in Human Skin*, The journal of clinical endocrinology & metabolism, 67, 373–378, 1988.

Webb, A. R., Slaper, H., Koepke, P. and Schmalwieser, A. W.: Know Your Standard: Clarifying the CIE Erythema Action Spectrum, Photochemistry & Photobiology, 87, 2, 483–486, 2011.

Xiang, F., Lucas, R., Hales, S., and Neale, R.: Incidence of nonmelanoma skin cancer in relation to ambient UV radiation in white populations, 1978-2012: empirical relationships, JAMA dermatology, 150, 1063–1071, 2014.

Zempila, M.-M., Giannaros, T. M., Bais, A., Melas, D., and Kazantzidis, A.: Evaluation of WRF shortwave radiation parameterizations in predicting Global Horizontal Irradiance in Greece, Renewable Energy, 86, 831–840, 2016a.

Zempila, M.-M., Koukouli, M.-E., Bais, A., Fountoulakis, I., Arola, A., Natalia, K., and Balis, D.: OMI/Aura UV product validation using NILU-UV ground-based measurements in Thessaloniki, Greece, Atmospheric Environment, 2016b.

Zerefos, C.: Evidence of the El Chichón stratospheric volcanic cloud in Northern Greece, Geofísica Internacional, 23, 1984.